



INVESTIGATION ON PHYSICO-MECHANICAL PROPERTIES OF GLASS-CERAMIC COMPOSITE FROM ECO-WASTE MATERIALS



This report is submitted in accordance with the requirement of the Universiti
Teknikal Malaysia Melaka (UTeM) for the Bachelor Degree of

اونيورسي تيكنيكل مليسيا ملاك
Manufacturing Engineering (Hons.)

UNIVERSITI TEKNIKAL MALAYSIA MELAKA

by

AFIFAH KHAIRINA BINTI ZUHAIMI



FACULTY OF MANUFACTURING ENGINEERING

2022

DECLARATION

I hereby, declared this report entitled “The Investigation on Physico-Mechanical Properties of Glass-Ceramic Composite from Eco-waste Materials” is the result of my own research except as cited in references.

Signature



Author's Name

AFIFAH KHAIRINA BINTI ZUHAIMI

Date

:25 JANUARY 2022

اونيورسيتي تيكنيكل مليسيا ملاك

UNIVERSITI TEKNIKAL MALAYSIA MELAKA

APPROVAL

This report is submitted to the Faculty of Manufacturing Engineering of Universiti Teknikal Malaysia Melaka as a partial fulfilment of the requirement for Degree of Manufacturing Engineering (Hons). The member of the supervisory committee is as follow:



ABSTRAK

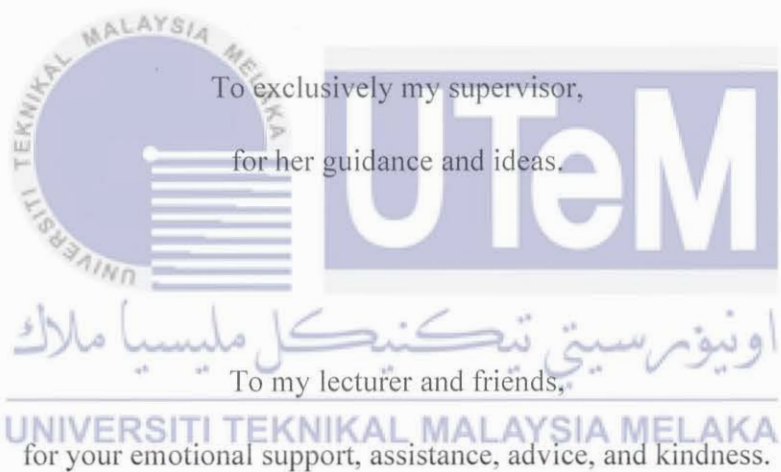
Tujuan kajian ini adalah untuk menyiasat kesan pemuatan pengisi daripada bahan sisa mesra alam terhadap sifat fiziko-mekanikal komposit kaca-seramik. Kulit kerang (KK) dengan saiz zarah sekitar $75\mu\text{m}$ telah digabungkan sebagai pengisi dalam komposit kaca-seramik sepanjang kajian ini. Sementara itu, kaca soda kapur silikat (SLSG) berfungsi sebagai matriks yang mempunyai saiz keseluruhan sekitar $75\mu\text{m}$. Pengisi KK telah dikeringkan dan dikalsinkan pada suhu 1000°C dengan kadar pemanasan malar $10^\circ\text{C}/\text{min}$ selama empat jam sebelum didedahkan kepada proses pensinteran terus. Empat kelompok rumusan dibuat dengan nisbah SLSG: CS 50:50, 60:40, 70:30 dan 100:0 wt.%. Untuk mencapai penyebaran seragam campuran, mesin pengisar bola telah digunakan untuk menggabungkan zarah. Bahagian segi empat sama hijau dibentuk dengan memampatkannya menggunakan penekan akapaksi pada 10 tan selama dua minit. Pada suhu 700 , 750 , 800 dan 850°C , sampel telah disinter dengan kadar pemanasan malar $2^\circ\text{C}/\text{min}$ dan tempoh tinggal selama satu jam. Untuk menentukan kehadiran ikatan hidrogen, *Fourier transformasi infrared spectroscopy* (FTIR) telah digunakan untuk mencirikan unsur KK, manakala X-ray Difraksi (XRD) dilakukan untuk mengenal pasti fasa komposit kaca SLS yang dikitar-semula. Sifat fizikal diukur menggunakan ASTM C373 sebelum keliangan lutsinar bagi komposit dianalisis. Kekerasan komposit SLSG kitar-semula dinilai menggunakan ujian kekerasan Vickers (ASTM C1327-99) dan ukuran akustik (ASTM E494-95), dengan peratusan ralat direkodkan untuk memerhatikan struktur mikro pada permukaan yang retak dan untuk membuat kesimpulan hubungan antara struktur mikro dan sifat fizikal dan mekanikal komposit SLSG. Dapatan menunjukkan bahawa sampel dengan 30wt.% pengisi KK mempunyai pengecutan linear yang tinggi dan keliangan ketara yang rendah, kedua-duanya menyumbang kepada ketumpatan pukal $2.09\text{g}/\text{cm}^3$. Corak XRD menunjukkan kuarza, kristalit, silikon oksida (SiO_2), kalsium oksida (CaO), dan natrium oksida (Na_2O) selepas proses pensinteran. Dalam ujian mikrokekeraan, komposisi ini mempunyai bacaan mikrokekeraan purata tertinggi iaitu 1004.86Hv.

ABSTRACT

The purpose of this study was to investigate the effect of filler loading from eco-waste material on physico-mechanical properties of the glass-ceramic composite. The cockle shell (CS) with a particle size of around $75\mu\text{m}$ was incorporated as a filler in a glass-ceramic composite throughout this study. Meanwhile, soda-lime silica glass (SLSG) served as a matrix having an overall size of around $75\mu\text{m}$. The CS filler was dried and calcined at temperatures of 1000°C with a constant heating rate of $10^\circ\text{C}/\text{min}$ for four hours before being exposed to the direct sintering process. Four batches of formulation were made with SLSG: CS ratios of 50:50, 60:40, 70:30, and 100:0 wt.%. To achieve uniform dispersion of the mixture, a planetary ball mill was employed to combine the particles. The green square part was formed by compacting it using uniaxial pressing at 10 tons for two minutes. At temperatures of 700 , 750 , 800 and 850°C , the samples were sintered with a constant heating rate of $2^\circ\text{C}/\text{min}$ and a dwell duration of an hour. To determine the presence of a hydrogen bond, Fourier transforms infrared spectroscopy (FTIR) was utilised to characterise the element of CS, while X-ray Diffraction (XRD) was performed to identify the phase of the recycled SLS glass composite. Before analysing the apparent porosity of the composite, the physical characteristics were measured using ASTM C373. The hardness of recycled SLSG composite was evaluated using the Vickers hardness test (ASTM C1327-99) and acoustic measurement (ASTM E494-95) where the percentage of the error will be recorded as comparison data. Scanning electron microscopy (SEM) was used to observe the microstructure of the surface fracture and concluded the relationship between microstructure and physico-mechanical properties of the SLSG composite. The findings revealed that the sample with 30wt. % CS filler had outstanding physical and mechanical qualities at 850°C . This formulation has a high linear shrinkage and a low apparent porosity, both of which contribute to its greater bulk density of $2.09\text{g}/\text{cm}^3$. XRD patterns indicated quartz, cristobalite, silicon oxide (SiO_2), calcium oxide (CaO), and sodium oxide (Na_2O) following the sintering process. The composition had the highest average microhardness reading, 1004.86Hv , in the microhardness test.

DEDICATION

To my beloved family,
for their compassion.



Thank You So Much.

ACKNOWLEDGEMENT

In the name of Allah, the most gracious, the most merciful, with the highest praise to Allah, I successfully completed the final year project without difficult situation. I am grateful to all of the people that have encouraged and inspired me to complete this project. I would like to personally thank everyone who has been involved in this research, directly or indirectly.

First and foremost, I would like to express my gratitude to my kind supervisor, Dr. Zurina binti Shamsudin from Faculty of Manufacturing Engineering at Universiti Teknikal Malaysia Melaka. Thank you so much for your valuable time, advice, feedback, suggestions, patience and guidance throughout this research. In addition, a huge thank you to all of the assistant engineers that have been involved in this project, for all the guidance, discussions and teachings during laboratory work.

اونيورسيتي تيكنيكل مليسيا ملاك

A special thank you also goes to my loved and respected parents and siblings for their encouragement, support, and prayers for the project's success. Finally, I would like to express my sincere to all of my friends, specifically my housemates, Ain, Athirah, Afiqah, Suhailah, Diana, Nabilah, and Faizin, and my classmates for their unending support.

Ultimately, I would like to thank everyone who helped with the preparation of this Final Year Project and deeply apologize for not being able to show my appreciation individually.

TABLE OF CONTENT

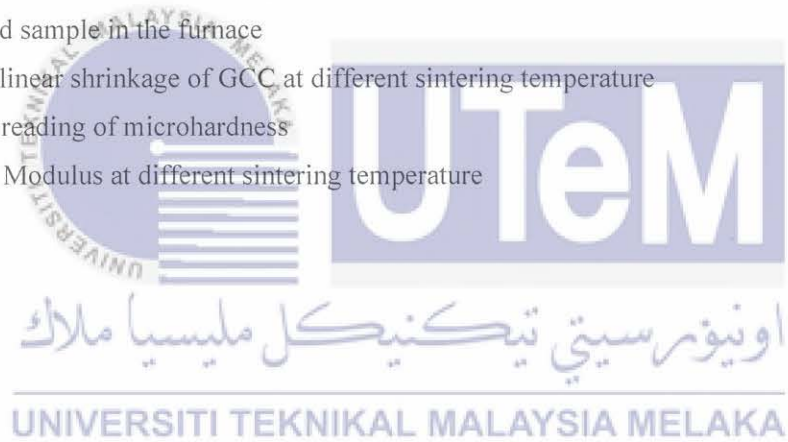
ABSTRAK	i
ABSTRACT	ii
DEDICATION	iii
ACKNOWLEDGEMENT	iv
TABLE OF CONTENT	v
LIST OF TABLES	viii
LIST OF FIGURES	ix
LIST OF ABBREVIATIONS	xi
LIST OF EQUATIONS	xiii
LIST OF SYMBOLS	xiv
CHAPTER 1 INTRODUCTION	1
1.1 Background of Study	1
1.2 Problem Statement	2
1.3 Objective	3
1.4 Scope of Study	3
1.5 Organization of Report	4
CHAPTER 2 LITERATURE REVIEW	5
2.1 Glass-Ceramic Composite (GCC)	5
2.2 Eco-material Waste as Raw Material in Processing Glass-Ceramic Composite	6
2.1.1 Soda-lime silicate (SLS) glass	6
2.1.2 Cockle Shell (CS)	8
2.3 Filler Load	9
2.3.1 Influence of Filler Load on Physico-mechanical Properties of GCC	9
2.4 Sintering Process	11
2.3.1 Type of Sintering Process	12

2.3.2	Factors Affecting the Sintering Process	13
2.3.3	Influence of Sintering Temperature on Physico-mechanical Properties of GCC	14
2.4	Properties Characterization	14
2.4.1	Fourier Transform Infrared Spectroscopy (FTIR)	14
2.4.2	Apparent Porosity	16
2.4.3	Linear Shrinkage	17
2.4.4	Bulk Density	17
2.4.5	X-Ray Diffraction (XRD)	18
2.4.6	Vickers Hardness Test	19
2.4.7	Acoustic Testing	20
2.4.8	Surface Morphology	22
CHAPTER 3 METHODOLOGY		27
3.1	Overview of Methodology	27
3.1.1	The Relation between Objectives and Methodology	27
3.1.2	Flow Chart for Process Planning	29
3.2	Preparation of Powder	30
3.2.1	Recycled Soda Lime Silicate Glass (SLSG)	30
3.2.2	Cockle Shell (CS)	32
3.3	Formulation of Batch	33
3.4	Mixing of Batch	34
3.5	Processing recycled soda-lime silica (SLS) glass and cockle shells (CS) composite	34
3.5.1	Forming Process	34
3.5.2	Process of Sintering Temperature	35
3.5	Characterization of CS powder	37
3.6	Characterization of GCC	38

3.6.1	Apparent Porosity, Bulk Density, and Linear Shrinkage	38
3.7	Characterization of sintered recycled SLS glass and CS composite	39
3.7.1	Identification of phase	39
3.8	Mechanical properties analysis	39
3.8.1	Microhardness Test	40
3.9	Acoustic Measurement	40
3.9.1	Ultrasonic Pulse Velocity	41
3.10	Morphology Analysis	43
3.10.1	Scanning Electron Microscope (SEM)	43
CHAPTER 4 RESULT AND DISCUSSION		44
4.1	Characterization of CS	44
4.2	The influence of different sintering temperatures on the characteristics of Glass-ceramic composite (GCC)	45
4.2.1	Physical Properties	45
4.2.2	Phase and Microstructure	50
4.2.3	Mechanical Property	52
4.2.4	Acoustic Measurement	53
4.3	Surface Morphology Analysis	54
CHAPTER 5 CONCLUSION & RECOMMENDATION		58
5.1	Conclusion	58
5.2	Recommendation	59
5.3	Life Long Learning Element	59
REFERENCE		61
APPENDICES		69
A	Gantt Chart for FYP 1	69
B	Gantt Chart for FYP 2	69

LIST OF TABLES

2. 1: Chemical Composition of SLS glass and ACS	7
2. 2 Batches of glass-ceramic composite	11
2. 3 The vibrational modes are assigned an FTIR spectral band	15
3. 1 The significance of methodology used in the study	28
3. 2 Formulation of batch	34
3. 3 Parameters for Sintering Process	37
4. 1 The colour differs as the sintering temperature changes.	46
4. 2 Overdried sample in the furnace	47
4. 3 Data for linear shrinkage of GCC at different sintering temperature	48
4. 4 Average reading of microhardness	53
4. 5 Young's Modulus at different sintering temperature	54



LIST OF FIGURES

2. 1 The Si-O-Si bond	6
2.2 Seashells dumped with the remaining meat	9
2. 3 The four fundamental components of materials in science and engineering	12
2. 4 The phase for the sintering process	12
2. 5 Analysis of FTIR for ASF-based glass-ceramics sintered at various sintering temperatures	16
2. 6 XRD pattern of foam-glass ceramics sintered for 60 minutes at different temperatures	19
2. 7 Technique for Ultrasonic Pulse-echo	22
2. 8 SEM micrographs of glass composite sintered at 800°C with varying egg shell contents (a) 5wt.% (b) 10wt.% (c) 15wt.% (d) 20wt.% [Indicator O – Open pore; C – Closed pore]	23
2. 9 SEM micrographs of glass composite sintered at 850°C with varying egg shell contents (a) 5wt.% (b) 10wt.% (c) 15wt.% (d) 20wt.% [Indicator: O – Open pore; C – Closed pore]	24
2. 10 FESEM micrograph of ASF bio-glass samples before sintered at B1:5wt. %, B2:10wt.%, B3:15wt.%, and B4:20wt.%	25
2. 11 Micrograph of glass-ceramic composite with 30wt.% of CS	26
3. 1 The Flow Chart for Process Planning	Error! Bookmark not defined.
3. 2 Clear glass bottle from household waste	30
3. 3 Size of crushed SLSG using a hammer	31
3. 4 Planetary Ball Mill used to crush the coarse particle into a fine particle	31
3. 5 Vibratory sieve shaker	31
3. 6 Size of 75µm of stainless-steel sifter	32
3. 7 Cockle shell waste	32
3. 8 CS in pestle and mortar	33
3. 9 Calcined CS in crucible container.	33
3. 10 Uniaxial Pressing	35
3. 11 Samples in Electric Furnace	36
3. 12 Sintering profile's schematic diagram	36
3. 13 Typical powder pattern	39
3. 14 Schematic of five indentations on sample.	40
3. 15 The EPOCH 650 Series Olympus Ultrasonic Flaw Detector	42
3. 16 Schematic of Ultrasonic Pulse Velocity Diagram	42
3. 17 7 Back Echoes and Initial Pulse	43

4. 1 FTIR spectra of calcined CS powder at 1000°C	44
4. 2 Pressed sample at 5 tonnes before the sintering process	46
4. 3 FTIR analysis of the shattered sample	47
4. 4 GCC's linear shrinkage at different sintering temperature	48
4. 5 The bulk density for every sample formulation at different sintering temperatures	49
4. 6 Apparent porosity at different sintering temperature	50
4. 7 XRD Analysis of the samples at a) 0wt.%, b) 30wt.% c) 40wt.% and d) 50wt.% of CS filler load	51
4. 8 SEM micrographs of glass composite sintered at 800°C with varying egg shell contents (a) 5wt.% (b) 10wt.% (c) 15wt.% (d) 20wt.% [Indicator: O – Open pore; C – Closed pore]	55
4. 9 SEM micrographs of glass composite sintered at 850°C with varying egg shell contents (a) 5wt.% (b) 10wt.% (c) 15wt.% (d) 20wt.% [Indicator: O – Open pore; C – Closed pore]	55
4. 10 FESEM micrograph of ASF bio-glass samples before sintered at B1:5wt. %, B2:10wt.%, B3:15wt.%, and B4:20wt.%	56
4. 11 Micrograph of glass-ceramic composite with 30wt.% of CS	57

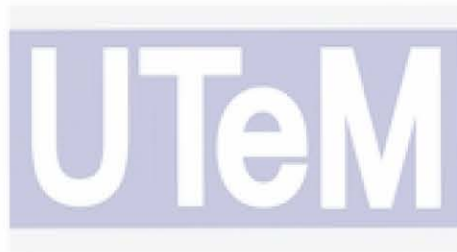


LIST OF ABBREVIATIONS

ACS	-	Ark Clamshell
Al ₂ O ₃	-	Aluminium Oxide
ASTM	-	American society for testing and materials
CaCO ₃	-	Calcium Carbonate
CaF ₂	-	Calcium Fluoride
CaO	-	Calcium Oxide
CS	-	Cockle shell
DT	-	Destructive Testing
ES	-	Eggshell
Etc.	-	Et cetera
Fe ₂ O ₃	-	Iron Oxide
FTIR	-	Fourier Transform Infrared Spectroscopy
GCC	-	Glass-ceramic Composite
GIC	-	Glass Ionomer Cement
Hv	-	Hardness Vickers
K ₂ O	-	Potassium Oxide
MgO	-	Magnesium Oxide
MnO	-	Manganese Oxide
Na ₂ O	-	Sodium Oxide
NDE	-	Non-destructive Evaluation
NDE	-	Non-destructive Examination
NDI	-	Non-destructive Inspection
NDT	-	Non-destructive Testing
P ₂ O ₅	-	Phosphorus Pentoxide
PE	-	Pulse-Echo
RM	-	Ringgit Malaysia
SEM	-	Scanning Electron Microscopy
SiO ₂	-	Silicon Dioxide
SLS	-	Soda-lime Silicate
SLSG	-	Soda-lime Silicate Glass



SO ₃	-	Sulphur Trioxide
SrO	-	Strontium Dioxide
TiO ₂	-	Titanium Oxide
TT	-	Through Transmission
TOFD	-	Time of Light Diffraction
UT	-	Ultrasonic Testing
WGC	-	Wollastonite glass-ceramic
XRD	-	X-ray Diffraction
ZnO	-	Zinc Oxide

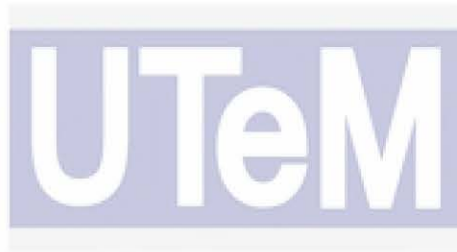


اونيورسيتي تيكنيكل مليسيا ملاك

UNIVERSITI TEKNIKAL MALAYSIA MELAKA

LIST OF EQUATIONS

2.1	Poisson's Ratio	16
2.2	Young's Modulus of Elasticity	16
2.3	Shear Modulus	16
2.4	Bulk Modulus	16
2.5	Known Longitudinal Velocity	16
3.1	Apparent Porosity	37
3.2	Bulk Density	37
3.3	Linear Shrinkage	37
3.4	Vickers Hardness	39
3.5	Longitudinal velocity	40
3.6	Young's Modulus	40



اونيورسيتي تيكنيكل مليسيا ملاك

UNIVERSITI TEKNIKAL MALAYSIA MELAKA

LIST OF SYMBOLS

%	-	Percentage
%AP	-	Apparent Porosity
θ	-	Angle
$^{\circ}$	-	Degree
$^{\circ}\text{C}$	-	Degree Celsius
$^{\circ}\text{C}/\text{min}$	-	Degree Celsius per minute
μm	-	Micron metre
Kg/m^3	-	Kilogram per metre cube
g	-	gram
g/cm^3	-	Gram per centimetre cube
mm	-	Millimetre
min	-	min
m/s	-	Metre per second
N/m^2	-	Newton per metre squared
wt.%	-	Weight Percentage



اونيورسيتي تيكنيكل مليسيا ملاك

UNIVERSITI TEKNIKAL MALAYSIA MELAKA

CHAPTER 1

INTRODUCTION

1.1 Background of Study

These days, urbanization and rapid industrial and lifestyle development contribute to an increase in the consumption of natural resources and a decrease in their availability (Jassim, 2017). On the contrary, humans have always produced trash and disposed of it in some fashion, which has an impact on the environment. As a result, the increased waste generated by industrial factories and human activities should be monitored. As a response, scientists have found new types of engineering, such as sustainable engineering and green engineering, to reduce energy and natural resource usage (Jassim, 2017). One of many ways in saving the environment is to reuse the waste from sustainable or eco-materials.

Soda-lime silicate glass (SLSG) as eco-material wastes generated from rapid industrial development are intensively used as alternative materials in the production of the glass-ceramic composite (Hossain et al., 2018). SLSG contributed smooth and non-reactive surfaces (Hasanuzzaman et al., 2016). It has greater physico-mechanical properties such as strength and fracture toughness than the parent glass if formed by melting and casting (Ingole et al., 2018) and heat treatment controlled. In this study, the glass-ceramic composite was formed using a sintering process. Eco-material waste such as cockle shells (CS) was used as the filler load in recycled soda lime silicate (SLS) glass-ceramic composite. Cockle Shells (CS) has shown potential to increase the strength of composite due to the presence of calcium oxide (CaO.)

Polycrystalline materials that were formed by the controlled crystallization of glass are defined as glass-ceramics (Pinckney, 2001). The glass-ceramic composite has better physical and mechanical properties (e.g., strength; fracture toughness) than the parent glass produced by melting and casting since it has a composite structure consisting usually of a fine crystalline phase scattered in a matrix of glass (Rahaman, 2014). Because of their strong

mechanical, chemical, and abrasion resistance, high hardness, variable thermal expansion depending on chemical composition, and sinterability to relatively high densities (92–98%) at temperatures usually less than 1000 °C, glass–ceramics can be a solution in many applications (Arcaro et al., 2017). To improve the strength properties of the glass-ceramic composite, filler material was added during the manufacturing of the glass-ceramic composite.

This study aims to investigate the effect of the addition of eco-waste materials on the properties of the glass-ceramic composite. The physical properties were tested using conventional measurement and the mechanical properties were evaluated using two different methods which are microhardness testing and acoustic method.

1.2 Problem Statement

The materials with a less hazardous substance, materials with a green environmental profile, or materials of higher recyclability can be classified as eco-materials. These eco-materials from wastes such as carbon fibres, glasses or from natural sources, for example, spent bleach earth, and cockle shells have potential that were explored as a filler to improve the performance of the product glass-ceramic composite using sintering process (Shamsudin et al., 2018). The glass-ceramic sample will be sintered at different temperatures ranging from 700 to 850°C (Ayooob et al., 2011; Gualberto et al., 2019).

A study by Jusoh et al., (2019a) has discussed that sintering temperature will affect the porosity, linear shrinkage, density, water adsorption and microstructure of the glass-ceramic composite. Influence the outcome of strength properties if poor densification causes high porosity. As the glass-ceramic is defined as polycrystalline materials, the strength is enhanced by decreasing their grain size. Hence, the formulation for the filler loading (wt.%) to improve the performance of the product glass-ceramic composite was investigated in this paper.

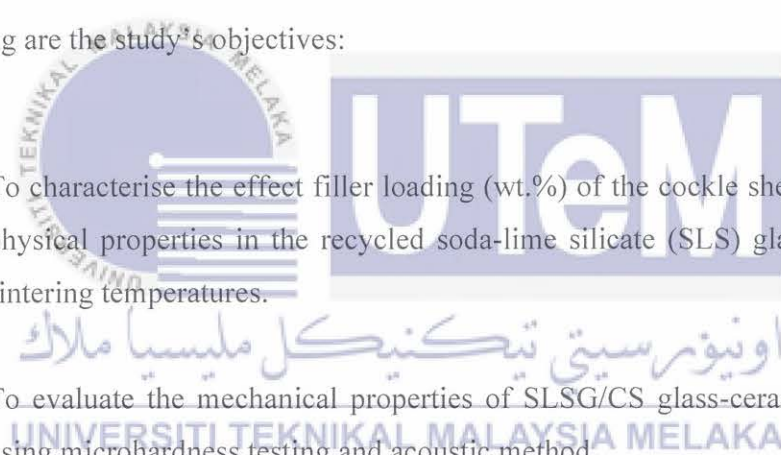
To measure one of the strength properties which is Young's Modulus, E for brittle materials, the common destructive test (flexural test) was used (Cattell et al., 2020). Regrettably, these features may not be dependable enough because the samples are performed on coupons, with the idea that the coupon is a true example of the component that would be used in services. That is why the results of the destructive test (flexural test) on

coupons may not apply to the component to be used in service, as it might be affected by the handling process.

As the result of the problem, this project focused on the fabrication of glass-ceramic composite from eco-waste materials. The mechanical property was evaluated via microhardness test and acoustic method. Non-Destructive Test (acoustic method) aided in predicting the failure probability of a component given the crack size and fracture toughness parameters of the materials (Sohn & Olivias-Martinez, 2014). The acoustic technique is used because it can recognize the thickness and the longitudinal velocity.

1.3 Objective

The following are the study's objectives:

- 
- (a) To characterise the effect filler loading (wt.%) of the cockle shells (CS) in the physical properties in the recycled soda-lime silicate (SLS) glass at different sintering temperatures.
 - (b) To evaluate the mechanical properties of SLSC/CS glass-ceramic composite using microhardness testing and acoustic method.
 - (c) To correlate the effect of filler loading on physico-mechanical to morphology from the literature review.

1.4 Scope of Study

The following are the study's scope of the study:

- a) The formulations of the filler loading (wt.%) of cockle shells (CS) are 30wt.%, 40wt.% and 50wt.% in the recycled soda-lime silicate (SLS) glass and cockle shells (CS) glass-ceramic composite sintered at different sintering

temperatures from 700°C, 750°C, 800°C and 850°C at a constant heating rate at 2°C/min and dwelling time for 1 hour.

- b) Calcination process of CS at 1000°C, characterisation of material via X-ray Diffraction (XRD) for phase identification and Fourier Transform Infrared Spectroscopy (FTIR) for detecting the hydrogen bond. Physical analysis of the recycled SLS glass and CS composite is determined using ASTM C373.
- c) Evaluate the mechanical properties on four (4) batches of the recycled soda lime silicate (SLS) glass and cockle shells (CS) composite using microhardness test according to ASTM C1327-99 and acoustic method (ASTM E494-95).

- d) Correlate the microstructure of cockle shells/recycled soda lime silicate (SLS) glass-ceramic composite with physico-mechanical properties using the literature review.

1.5 Organization of Report

This study is divided into five chapters: introduction, literature review, methodology, result and discussion, and conclusion. The first chapter discussed the background of the study, problem statement, objectives, and scopes of the study. The second chapter's literature review includes past research or study on glass-ceramic composite, SLSG, CS, sintering process and parameters affecting sintering, microhardness testing and acoustic testing. The third chapter covers the entire flow of the study, methodologies, and procedures that will be used to finish this research. In the fourth chapter, the information collected after completing several selected tests such as the Vickers hardness test, bulk density, linear shrinkage, and apparent porosity were examined. Conclusions and recommendations from this study are presented in chapter five.

CHAPTER 2

LITERATURE REVIEW

This chapter discussed reviews study based on earlier research by other scholars. The goals of this chapter are to learn more about prior studies that were relevant to this paper and can be used to support this study to reach the best conclusion for this paper. This chapter discussed the studies about eco-material waste as filler for recycled soda lime silicate (SLS) glass-ceramic composite, destructive test (Flexural test) and non-destructive testing (ultrasonic technique). From the methodological step through the completion of PSM 2, this chapter guided the planning process of the entire project.

2.1 Glass-Ceramic Composite (GCC)

Glass-ceramics are ceramic materials made from the nucleation and crystallization of glass under controlled conditions. Glass-ceramics could also offer substantial advantages over standard glass or ceramic materials by combining the flexibility of glass forming and inspection with better and frequently unique glass-ceramic characteristics (Pinckney, 2001). Deubener *et al.*, (2018) proposed the updated definition of glass-ceramics, which glass-ceramics are inorganic, non-metallic materials prepared by controlled crystallization of glasses via different processing method.

Efficient nucleation, which allows the formation of small, randomly oriented grains without voids, micro-cracks, or other porosity, is the core of regulated internal crystallization (Höland & Beall, 2019). Pinckney (2001) stated that the important variables in the creation of a glass-ceramic are glass composition, glass ceramic phase assembly, and microstructure crystalline. Due to the speedy development of the glass ceramics, researchers aiming to improve the mechanical properties of glass ceramic by integrating recycled glass with

natural waste material (Chinnam et al., 2013). There are various types of glass-ceramic applications such as technical applications, consumer applications, optical applications, medical and dental applications, electrical and electronic applications, architectural applications, coatings and solders, and glass-ceramics for energy applications (Höland & Beall, 2019).

2.2 Eco-material Waste as Raw Material in Processing Glass-Ceramic Composite

Sustainable materials are those employed in the consumer and industrial economies that can be produced in sufficient quantities without depleting non-renewable sources or upsetting the environments and critical natural resource systems established steady-state balance. The eco-material wastes such as soda-lime silicate glass and cockle shell are used in this study.

2.1.1 Soda-lime silicate (SLS) glass

For hundreds of years, soda-lime glass, also called soda lime silicate (SLS) glass has been manufactured throughout most of Europe. Silica, mostly in the shape of sand, and limestone were plentiful almost everywhere. Crown glass can be another term for a high-silica variety of soda lime which had been used for window. The SLS glass is made up of silicone-oxygen tetrahedron (SiO_4) connected at the oxygen atoms (Karazi et al., 2017). As seen in Figure 2.1, the chemical ordering is quite strong; each silicon atom is coupled to four oxygen atoms, and each oxygen atom is shared by two silicon atoms.

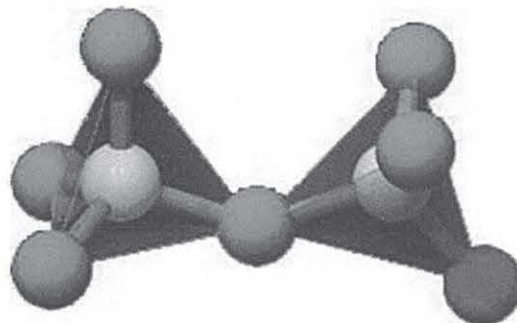


Figure 2. 1: The Si-O-Si bond (Karazi et al., 2017)

Karazi et al., (2017) claimed that soda-lime silicate is reasonably easy to melt and make, chemically resistant, and affordable. Because of its workability and affordability, this type of glass can be used in a wide range of things, including window panels, bottles and vessels for food, beverages, and commodity products, as well as light bulbs and art and design pieces. The SLS glass has been used as a material in processing glass-ceramic composite.

SLS glass waste has the potential as a building material in glass ionomer cement (GIC) production (Francis Thoo et al., 2013; Khiri et al., 2020). GICs are broadly employed in a variety of clinical applications, including posterior and anterior tooth fillings, luting agents, sealants, linings, orthodontic bracket cement, root canal fillings, and so on (Francis Thoo et al., 2013). In addition, SLS glass waste is also used to fabricate foam glass-ceramics (Hisham et al., 2021). The traditional solid-state sintering process was used to successfully create a series of 1 and 6 wt.% foam glass-ceramics at varied sintering temperatures for 60 minutes. Hisham *et al.*, (2021) obtained the lowest density (1.014 g/cm^3) of the samples with maximum expansion (62.31 %) at 6 wt.% of ark clamshell (ACS) content sintered at 800°C for 60 minutes. The chemical composition of SLS glass and ACS raw materials that has been analysed can be seen in Table 2.1 below.

Table 2.1: Chemical Composition of SLS glass and ACS (Hisham et al., 2021)

Oxides (wt%)	Raw Materials	
	SLS ± 0.1	ACS ± 0.1
SiO ₂	71.90	0.43
CaO	11.69	53.41
Na ₂ O	13.00	0.68
Al ₂ O ₃	1.39	-
MgO	1.43	0.18
K ₂ O	0.15	-
P ₂ O ₅	0.05	0.06
SO ₃	0.15	0.08
Fe ₂ O ₃	0.15	0.04
ZnO	0.03	0.05
SrO	0.01	0.14
Others	0.05	45.23
Total	100	100

2.1.2 Cockle Shell (CS)

The aquaculture sector is one of Malaysia's most important sector due to the strategic location, which allows for easy access to a protein source from the sea. Seashell waste such as cockle shells, oyster shells, mussel shells and scallop shells, among others, comes from the aquaculture sector and is available in large amounts in some areas, where it is frequently thrown or end up in landfills with no re-use value (Mo et al., 2018).

Cockle, formally known as *Anadara granosa*, are a type of indigenous bivalve mollusc that may be found in the coastal areas of Southeast Asia, mainly Malaysia, Thailand, and Indonesia (Sahari & Mijan, 2011). In 2019, 23.89 metric tonnes of cockles worth RM3.2 million were harvested, compared to 1,200 metric tonnes worth RM10.69 million harvested last year (Dermawan, 2021).

The information above can be used to determine how many waste shells are produced. In Figure 2.2 below, it shows that the seashells are dumped with the remaining meat in landfills (Barros et al., 2009). The shells that have been discarded and left untreated may generate an awful smell and an unpleasant sight in the area (Mohamed et al., 2012) due to the degradation of the leftover flesh in the shells or the microbial decomposition of salts into gases like H_2S , NH_3 , and amines (Yoon et al., 2003).

Studies by Hazurina *et al.*, (2012), Muthusamy *et al.*, (2012), and Mo *et al.*, (2018) have stated that this situation can be avoided by recycling the cockle shells as an alternative partial cement in concrete due to the composition of the cockle shells. (Barros et al., 2009) indicated that seashells are highly developed and used in other nations for a variety application. The rich calcium carbonate ($CaCO_3$)-based shells of the cockle provide an appealing substitute material that is inexpensive, readily available, and abundant for use in the manufacture of calcium-based bone grafting materials (George et al., 2019). In addition, the cockle shells can be used as a filler loading in fabricating glass-ceramic composite (Shamsudin et al., 2018) and thermoplastic composite (Munusamy et al., 2019).

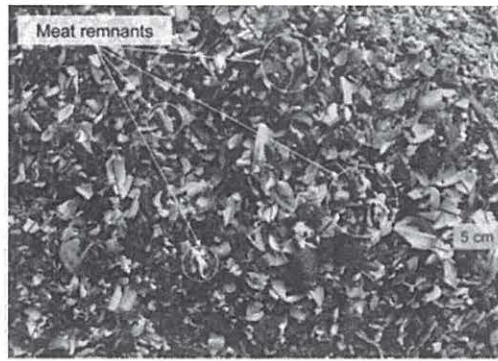


Figure 2.2: Seashells dumped with the remaining meat (Barros et al., 2009)

The cockle shells are made up of 96% calcium carbonate (CaCO_3), with organic compounds and other oxides including silicon dioxide (SiO_2), magnesium oxide (MgO), and sulphur trioxide (SO_3) making up the rest (Mohamed et al., 2012). The world's supply of calcium carbonate is currently almost entirely obtained from limestone mining, which has been deemed damaging and harmful to the environment (Wang et al., 2019). There are three polymorphs that included in calcium carbonate (CaCO_3), which are calcite, aragonite, and vaterite (George et al., 2019).

2.3 Filler Load



Wypych (2016) discussed that the definition for the filler load must be simple and precise, so that people can understand the definition. Wypych defined the filler as a solid material that can change the physical and chemical properties of materials through surface interaction or lack thereof, and via its own physical properties. One of the primary goals of filler addition is to improve mechanical qualities at a lower cost (Onuoha et al., 2017).

2.3.1 Influence of Filler Load on Physico-mechanical Properties of GCC

Kim *et al.*, (2002) stated that the filler loading influences flexural strength and modulus, hardness, and fracture toughness of a composite. This statement is supported by Mark *et al.*, (2020) as filler load is found to improve the yield strength, tensile modulus,

flexural strength, flexural modulus, and hardness of polypropylene as the value of filler loading increased.

A study by Mesri *et al.*, (2020a) employed eggshell (ES) waste and bentonite as filler material, whereas, SLSG, spent bleach earth (SBE) and borosilicate glass (BSG) as the matrix. The composites were sintered for an hour at four different sintering temperatures, 750°C, 800°C, 850°C, and 900°C, at a heating rate of 2°C/min. The powder has a particle size around 40µm. Uniaxial dry pressing is utilised to formed the samples at five various filler loading (wt.%) of ES and bentonite loading, which are 2wt.%, 5wt.%, 10wt.%, 15wt.%, and 20wt.%. High filler loading of eggshell waste sintered at 900°C resulted in the lowest water absorption of 2.48%, along with a 6.25% apparent porosity and a bulk density 2.52 g/cm³.

Another study that has been carried out by Noor *et al.*, (2015) also used eggshell waste and soda-lime silicate glass as the materials to make new CaSiO₃, wollastonite glass ceramics (WGC) materials due to CaO and SiO₂ resources. The powder particle size for ES and SLS glass composite is around 63 µm. The mixture that consists of 15 wt.%, 20 wt.% and 25 wt.% of CaO obtained from EG and 85 wt.%, 80 wt. % and 75 wt.% of SLS glass powder, respectively, were mixed in the rotary ball mill for 24 hours to create a homogeneous powder mixture. Pellets of the mixture are formed by blending the powder mixture with the organic binder polyvinyl alcohol (PVA). The 13 mm diameters pellets are sintered at three different temperatures, namely 800°C, 900°C, and 1000°C for 120 minutes each. The batches of the glass-ceramics are displayed in Table 2.2 below. As a comparison, one pellet from each batch will be left at ambient temperature.

Every batch of the glass-ceramic for the sample S1 consists of 15wt.% of ES powder and 85wt.% of SLS glass, whilst sample S2 has 20wt.% of ES powder and 80wt.% of SLS glass and sample S3 has 25wt.% of ES powder and 75wt.% of SLS glass. Archimedes principle is applied to determine the density of each WGC pellet, and the X-Ray Fluorescence (XRF) measurement was carried out with a Shimadzu Energy Dispersive X-ray Spectrometer model EDX-270. To evaluate the structure of each WGC sample, the Philips X-ray (Model pw 1380) is utilised. X'Pert Highscore programme is used to collect the acquired results. The samples had densities of approximately 2.5g/cm³ at room temperature, 27°C, closer to density of the SLS glass. The densities of samples S1, S2, and S3 increased in the range of 2.7g/cm³ at 800°C sintering temperature, 2.9 g/cm³ at 900°C,

and roughly 3.0 g/cm^3 at 1000°C because the WGC samples sintered at higher temperatures, ranging from 800°C to 1000°C .

Table 2. 2: Batches of glass-ceramic composite (Noor et al., 2015)

Sample Code	Filler Loading (wt.%)	
	ES	SLS glass
S1	15	85
S2	20	80
S3	25	75

Shamsudin *et al.*, (2018) used recycled soda-lime silicate glass (SLSG) waste and cockle shells (CS) for producing the GCC. The cockle shell filler is dried at 100°C for 24 hours in drying oven and calcined at temperatures of 800°C and 1000°C before being exposed to the direct sintering process. The powder particle size for recycled SLSG and CS are $75\mu\text{m}$. The formulation of the filler loading for the composite is 30wt.%, 40wt.%, and 50wt.% for CS and 70wt.%, 60w.%, and 50wt.% for recycled SLSG. The composite is sintered at fixed sintering temperature at 800°C with a constant heating rate at $2^\circ\text{C}/\text{min}$ for 60 minutes dwelling time.

Based on the result of apparent porosity, it has been discovered that apparent porosity is proportional to filler loading. The lowest percentage of apparent porosity is 3.62%.

2.4 Sintering Process

Sintering is a thermal energy-based manufacturing technique for producing density-controlled materials and components from metal or ceramic powders (Kang, 2005). As a result, sintering is classified as part of the synthesis/processing element of materials science and engineering, which can be seen in Figure 2.3. As material synthesis and processing have become increasingly important in recent years for material development, the importance of sintering as a material processing method is growing. Sintering process will cause material densification, which results in components with improved mechanical, thermal, and electrical properties (Van Nguyen et al., 2016). Sintering intends to manufacture sintered objects with reproducible and, if possible, specified microstructures by controlling sintering factors. Controlling grain size, sintered density, and the size and distribution of other phases,

including pores, is referred as microstructural control. The ultimate goal of microstructural management is to construct a fully dense body with a fine grain structure.

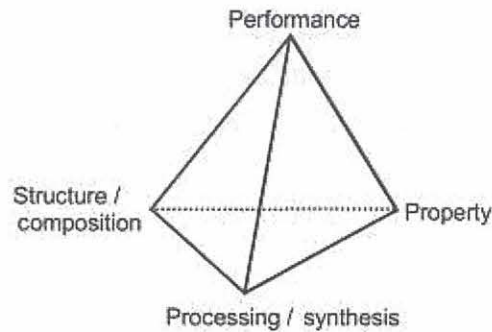


Figure 2. 3: The four fundamental components of materials in science and engineering (Kang, 2005)

2.3.1 Type of Sintering Process

Sintering process are broadly classified into two types: solid state sintering and liquid phase sintering. For solid state sintering, it tends to happen when the powder compact is entirely densified in a solid state at the sintering temperature, whereas liquid phase sintering occurs when a liquid phase is noticeable in the powder compact all through sintering. The schematic phase diagram in Figure 2.4 depicts the two types of sintering process. Solid state sintering occurs in an $A-B$ powder compact with composition X_1 at temperature T_1 , however liquid phase sintering happens in the identical powder compact at temperature T_3 (Kang, 2005). Kang (2005) also mentioned that there are other types of sintering, such as transient liquid phase sintering and viscous flow sintering.

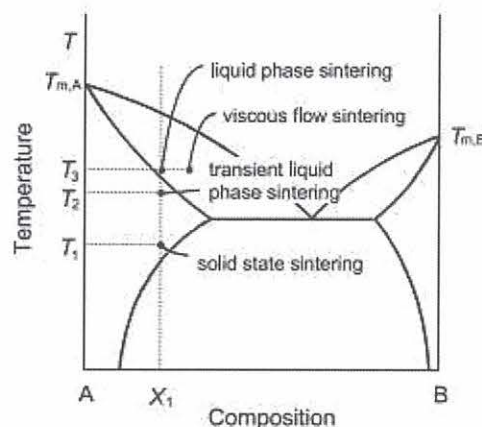


Figure 2. 4: The phase for the sintering process (Kang, 2005)

2.3.2 Factors Affecting the Sintering Process

There are two types of significant variables that influence sinterability and the sintered microstructure of a powder compact: material variables and process variables. The raw material factors (material variables) comprise the chemical composition of the powder compact, powder size, powder form, powder size distribution, degree of powder agglomeration, and so on. These characteristics have an impact on the powder's compressibility and sinterability (densification and grain growth). The uniformity of the powder combination is especially important in compacts comprising more than two types of powders. Not only mechanical milling but also chemical processing, such as sol-gel and coprecipitation techniques, have been explored and used to increase homogeneity. Many factors can influence the sintering properties, the most significant factors are the properties of the powder, the forming circumstances, and sintering conditions. The elements for sintering conditions consist of sintering temperature and time, heating rate, cooling rate, sintering environment, and sintering pressure. The porosity, density, strength, and hardness of the sinter are all affected by the sintering temperature and time. When the sintering temperature is too high and the time is too long, the performance suffers, and there may even be an over-burning defect.

2.3.3 Influence of Sintering Temperature on Physico-mechanical Properties of GCC

Saparuddin et al., (2020) conducted a study using SLS glass and ES waste to synthesize foam glass-ceramic. The powder particle average size for SLS glass and ES waste is 45 μ m. A digital analytical balance is utilised to weigh both of the powders. Then, both of the powders were put into the mortar using the empirical formula (6 % ES and 94% SLS glass powder) and ground for 10 to 15 minutes to obtain a homogeneous powder. The powder was then pressed into pellet form using a hydraulic pressing machine with a diameter of 13 mm and a thickness of 2 mm with an applied force of 5 MPa. An electric furnace is used to sinter all pellet samples at three different sintering temperatures, which are 700°C, 800°C, and 900°C for 1 hour at a heating rate of 10°C/min. The pellets were ground into a fine powder after the sintering process for further analysis.

There is a linear relationship between 0 % and 0.3 % compressive strain at 700°C of sintering temperature, showing that is the elastic area. After being sintered at 800°C for 60 minutes, the samples had a maximum porosity of 83.6 % and a minimum density of 0.421 g/cm³. At 700° sintering temperature, the greatest compressive strength is 1.82 MPa and the lowest is 0.42 MPa. The technique resulted in changes in the foam-glass ceramics sample at 900°C, which improved to 1.06MPa.

2.4 Properties Characterization

Fourier Transform Infrared Spectroscopy (FTIR), apparent porosity, linear shrinkage, bulk density, X-ray diffraction (XRD), Vickers hardness test, acoustic test, and glass-ceramic surface morphology were all employed in this study. The properties and the characteristics of the sintered glass-ceramic composite were investigated.

2.4.1 Fourier Transform Infrared Spectroscopy (FTIR)

The Fourier Transform Infrared Spectroscopy (FTIR) technique is used to get the absorption, emission, and photoconductive infrared spectra of solids, liquids, and gases

(Sindhu et al., 2015). Distinct functional groups that existed in the samples at different temperatures is shown in the FTIR result in Figure 2.6, whereas Table 2.3 showed the assignment of vibrational modes based on different wavenumbers. Jusoh et al., (2019b) reported the existence of Si-O-Si bending and stretching modes with wavenumbers in the range of $\sim 860\text{--}940\text{ cm}^{-1}$ and $\sim 1020\text{ cm}^{-1}$, respectively, in all sintered samples at different temperatures corroborated the presence of silica in SLS glass powder. The presence of a P-O bending mode bond and asymmetric P-O-P bond in samples sintered at 600, 800, 1000, and 1200°C showed the production of a crystallisation Ca-P phase in the ASF glass-ceramics composition during the sintering process. When the sample was treated to 1000°C , the production of the Ca-P phase in FTIR spectra and needle-like crystals in the FESEM micrograph confirmed the formation of the fluorapatite crystal phase.

A study by Shamsudin et al., (2019) used FTIR to evaluate the tested samples, and the hydrogen bond affecting the densification of the recycled SLSG and CS composite is proven. All sintered samples are calcined to produce a better outcome, and no cracks are discovered by eye inspection. Regrettably, samples without calcination and the addition of filler loading (wt.%) of cockle shell filler rose from 30wt.% resulting in crack formation among samples of composite with 40wt.% and 50wt.% of CS filler loading. Because the absorption water molecules were still trapped and the result is displayed from the hydrogen bond in the FTIR spectrum, this behaviour is predictable.

Table 2. 3: The vibrational modes are assigned an FTIR spectral band (Jusoh et al., 2019b).

Wavenumbers (cm^{-1})	Assignment of vibrational mode
$\sim 415\text{--}540$	Si—O—Si bending mode
$\sim 550\text{--}560$	P—O bending mode
$\sim 720\text{--}760$	Symmetric P—O—P bond
$\sim 860\text{--}940$	Si—O—Si stretching mode
~ 1020	Si—O—Si stretching mode
$\sim 1400\text{--}1500$	C—O stretching mode

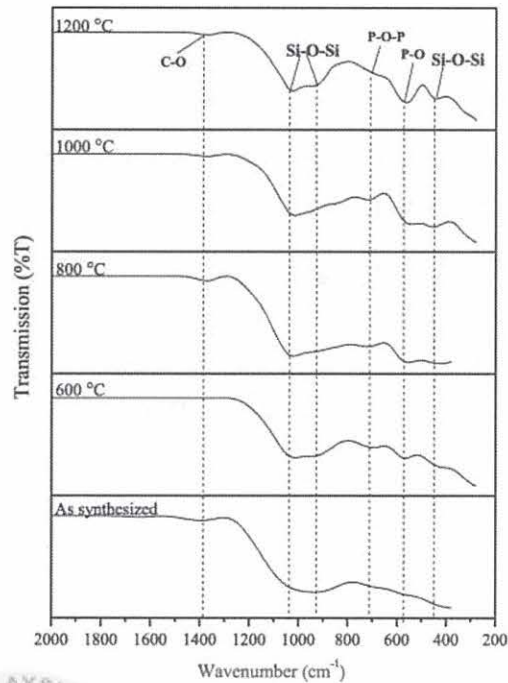


Figure 2. 5: Analysis of FTIR for ASF-based glass-ceramics sintered at various sintering temperatures (Jusoh et al., 2019b)

2.4.2 Apparent Porosity

Guan et al., (2016) revealed that the initial porosity and particle size distribution impact the rate of porosity decline with sintering time. The greater the difference in initial porosity and particle size distribution, the slower the reduction in porosity rate. The study by Mesri et al., (2020b) stated that the apparent porosity is calculated after 24 hours of soaking. In a broad sense, as the sintering temperature increased, the apparent porosity decreased. At 0wt.% of ES filler loading, apparent porosity decreases from 17.95% to 12.97%. The apparent porosity is decreased from 18.89% to 14.13% when the filler loading is increased to 5wt.%. At 10 wt.%, apparent porosity decreases from 21.26% to 14.38 %. On the other hand, higher sintering temperatures have an impact on apparent porosity because the optimum viscous flow has the potential to seal the porosity.

2.4.3 Linear Shrinkage

Hisham *et al.*, (2021) compared foam glass-ceramics with different compositions generated from ark clamshell (ACS) and soda-lime silica glass (SLSG) bottles sintered at different sintering temperatures. According to the study, when the ACS content and sintering temperature increase, the linear shrinkage and total porosity decrease, and therefore the results using the field emission scanning electron microscope are trustworthy (FESEM). Yang *et al.*, (2016) concluded that linear shrinkage does not increase as the sintering temperature increases. With increasing retention time, the initial shrinkage temperature ratio gradually decreases.

2.4.4 Bulk Density

Almasri *et al.*, (2017) reported that forming of glass-ceramics increases the density of the glass's fundamental structure. The increase in the overall density of the sample might be due to the formation of crystals on the glass. The crystallization process also leads to an increase in density. As the bonding develops during crystallisation, the particles are reorganised, the bond flow generates sintering, and the particles are shaped by the sintering neck. This has a slightly positive impact in terms of decreasing the pore size of the glass-ceramic sample, resulting in particle aggregation and an increase in density.

The investigation on glass-ceramic from the industrial residue by Chinnam *et al.*, (2015) concluded that the density of glass-ceramic composite decreases significantly as the sintering temperature increases. When sintered at 700 and 800 °C, the bulk density of foam glass-ceramics was reduced from 0.682 to 0.421 g/cm³. Saparuddin *et al.*, (2020) stated that the trend of the bulk density determined the advancement of porosity. The trend was reversed when the sample was sintered at 900 °C when the density of the sample increased to 0.565 g/cm³.

2.4.5 X-Ray Diffraction (XRD)

XRD is used to identify the crystalline phase for ASF glass-ceramics. The sample that was synthesised represents the sample that did not go through the sintering process after being quenched. (Jusoh et al., 2019b) reported that for different sintering temperatures, three peaks are seen in ASF-based glass ceramics, which pertain to fluorapatite ($\text{Ca}_5(\text{PO}_4)_3\text{F}$, 98-001-7206), mullite (Al_2SiO_5 , 98-002-3557), and anorthite ($\text{Ca}(\text{Al}_2\text{Si}_2\text{O}_8)$, 98-000-6200). As the samples were sintered at 600 °C and 800 °C, the amount of fluorapatite phase increased. Once the sample was heated to 1000 °C, mullite phase growth with most fluorapatite phases was detected. Fluorapatite and anorthite are the crystal phases in ASF glass-ceramics at a sintering temperature of 1200 °C. Fluorapatite exhibits the highest intensity phase of the diffraction peak, and the intensity of the peak increased with increasing sintering temperature. Furthermore, as the sintering temperature increased, the fluorapatite peaks increased, and the formation of the fluorapatite phase became optimal because energy was supplied throughout the sintering process.

The XRD pattern of the composite sintered at various temperatures is depicted in Figure 2.6. At 750°C, several peaks with defective crystalline structures began to develop, indicating the presence of albite, quartz, and diopside crystals. The addition of niobium oxide aided in the creation of crystalline structures, verifying the manufacture of glass-ceramics at temperatures ranging from 650 to 750°C. (Saparuddin et al., 2020) has discussed that with an increase in sintering temperature to 800 °C, there was an appearance of cristobalite (SiO_2 , 96-900-9688) and the growth of wollastonite (CaSiO_3 , 96-900-5778), whereas, at 900 °C, there was a significant increase in the peak of wollastonite (CaSiO_3 , 96-900-5778) as well as the growth of cristobalite.

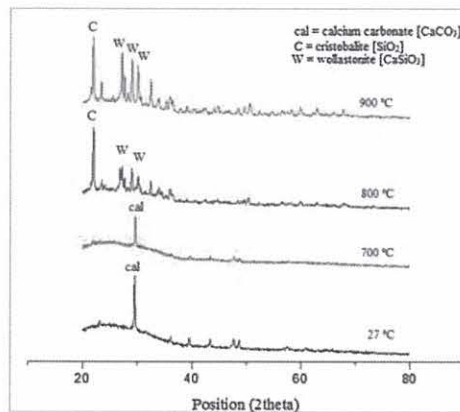


Figure 2. 6: XRD pattern of foam-glass ceramics sintered for 60 minutes at different temperatures (Saparuddin et al., 2020)

XRD is used to identify the crystalline phases present in the treated sample of cockle shell filler and composite, it was discovered that CaO completely precipitated when the calcination temperature is increased to 1000°C, and quartz phases predominated at high volume glass content. The XRD finding for sintered glass waste composite reveals a prominent peak at 36.14 ° of 2θ, indicating the presence of high-intensity quartz (JCPDS card81-65) solid solution. Because of the primary structure of both cockle shells and glass, the quartz phase can be determined. The appearance of the quartz phase with high intensity was identified in all samples at the diffraction peak between 20° and 40°.

Mesri et al., (2020b) reported that the XRD study demonstrated that quartz first precipitated and that when the SBE loading increased to 25% wt., phases coesite, cristobalite, and carnegite precipitated as well. Meanwhile, Noor et al., (2015) procured the XRD results of WGC samples that revealed the pattern of wollastonite's crystalline phase at temperatures above 900°C.

2.4.6 Vickers Hardness Test

Ben Ghorbal *et al.*, (2017) defined the Vickers hardness test as a hardness test that involves driving a diamond indenter in a rectangular base pyramid with a calibrated machine. After loading the sample, the diagonal of the produced print is measured. To measure mechanical properties such as hardness, modulus of elasticity, tensile properties, bulk material toughness, and ceramic coating adhesion, the traditional indentation test, which is the Vickers hardness test.

Before performing the Vickers hardness test, several things must be addressed. For example, the sample must be small enough to fit on the scale, and the sample surface must be smooth to acquire an accurate impression and prevent mistakes during testing (ben Ghorbal et al., 2017). The finding by Zawrah *et al.*, (2017) stated that during the sintering process, the random orientation and entanglement of the resulting phase crystals in the glass matrix distorts or weaken the fraction. The generated crystals drive the inner thin layer and the outer coarse layer in the glass matrix, resulting in residual stress and improved flexibility and absorption.

2.4.7 Acoustic Testing

The transmission of high frequency sounds into a material to interact with elements within the substance that reflect or attenuate it is referred to as ultrasonic testing. Ultrasonic testing is classified into three types: pulse-echo (PE), through transmission (TT), and time of flight diffraction (TOFD). The result of flexural testing on ceramic materials is dependent on sample preparation, which includes multiple handling processes. According to Wowk *et al.*, (2018) the problem with composite materials is determining how coupon testing can be utilised to derive properties that can be used for design and analysis rather than just quality control. As a result, the ultrasonic technique is utilised to authenticate the coupon testing result from the flexural test, indicating that the coupon testing result is appropriate for usage in services or products.

ASTM E494-95 acts as a practical reference in the use of NDT procedures measuring ultrasonic velocity in composite materials/structures. Ultrasonic velocities can be used to determine the modulus of elasticity or Young's modulus of materials, monitor the progression of thermal shock damage, define indirectly fracture toughness, R-curve behaviour, hardness depending on heat treatment, volume fraction porosity, and density (Phani, 2007). Ultrasonic evaluation methods such as A-scans, B-scans, and C-scans can be used to investigate various sorts of flaws in ceramic materials. A-scans display will be used to present the findings from the typical ultrasonic pulse-echo defect detection equipment in ASTM E494-95.

Moghanizadeh (2021) claimed that ultrasonic wave is associated with elastic constants and material's density. Seeing as different materials have distinct elastic constants,

products made of different materials can be differentiated by measuring their elastic constants. Furthermore, the elastic constants of materials can be calculated by measuring the velocity of longitudinal and transverse waves (Moghanizadeh & Farzi, 2016). Moghanizadeh also stated that material elastic constants are related to fundamental solid-state phenomena such as specific heat interatomic forces, co-ordination changes, and so on, along with impact shock, fracture, porosity, crystal growth, and microstructural factors such as grain shape, grain boundaries, texture, and precipitates etc. As a result, investigating the propagation of ultrasonic vibrations in materials is a clever method for determining elastic constants, which gives data to differentiate different materials from one another. The calculation of longitudinal and transverse wave velocities in an isotropic material allows the elastic constants to be approximated using the following formula in Equation 2.1 until Equation 2.4 (ASTM E494-95)(*ASTM E494 - 95 Standard Practice for Measuring Ultrasonic Velocity in Materials*, n.d.).

In which σ is the Poisson's ratio and E , G , and K are the Young's Modulus, transverse, and bulk modules. The ultrasonic longitudinal and transverse wave velocities are denoted by V_l and V_s , respectively. The equations below are commonly used for material characterization using ultrasonic wave velocity measurements, as well as for evaluating the effect of metallurgical characteristics such as precipitation on metals in isotropic materials (*ASTM E494 - 95 Standard Practice for Measuring Ultrasonic Velocity in Materials*, n.d.).

Measuring ultrasonic velocity entails determining the time of travel between the first and second back surface reflections and dividing it by the distance travelled by ultrasound, as displayed in Figure 2.7 below. The accuracy of these measurements is determined by the precision with which time of travel and component thickness are measured (Murayama et al., 2004). For measuring longitudinal velocity, a standard beam probe should be utilised. The value of known longitudinal velocity in the test specimen shall be computed as the Equation 2.5 below, where A_k is the distance, m, measured along the baseline of A-scan display from the first to the N th back echo, n_l is the number of round trips, unknown material, t_l is the thickness of unknown material in m, v_k is the velocity in known material, m/s, A_l is the distance from the first to the N th back echo on the unknown material, m, measured along the baseline of the A-scan display, n_k is the number of round trips, and t_k is the thickness of known material. Similarly, the unknown transverse velocity (V_s) can be calculated by comparing the transit time of a transverse wave in an unknown material to the transit time

in a known material (V_l). The measurements must be performed in the same manner as indicated for the longitudinal wave.

$$\sigma = \frac{((1 - 2) \left(\frac{V_s}{V_l}\right)^2)}{2x(1 - \left(\frac{V_s}{V_l}\right)^2)} \quad \text{Equation 2. 1}$$

$$E = \frac{\rho V_s (3V_l^2 - 4V_s^2)}{V_l^2 - V_s^2} \quad \text{Equation 2. 2}$$

$$G = \rho V_s^2 \quad \text{Equation 2. 3}$$

$$K = \rho \left(V_l^2 - \frac{4}{3(V_s^2)} \right) \quad \text{Equation 2. 4}$$

$$V = \frac{(A_k n_l t_l v_k)}{(A_l n_k t_k)} \quad \text{Equation 2. 5}$$

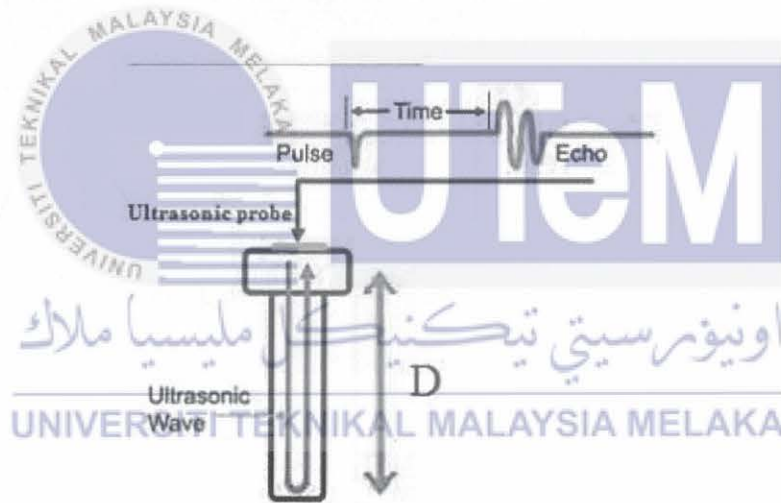


Figure 2. 7: Technique for Ultrasonic Pulse-echo (Moghanizadeh, 2021)

2.4.8 Surface Morphology

Surface morphology and topography are essential features of glass-ceramic materials (from the nano to the macro scale) that are derived from chemical properties/structures and fabrication methods (Popelka et al., 2020). The surface morphology can be carried out using scanning electron microscopy (SEM) and field emission scanning electron microscopy (FESEM).

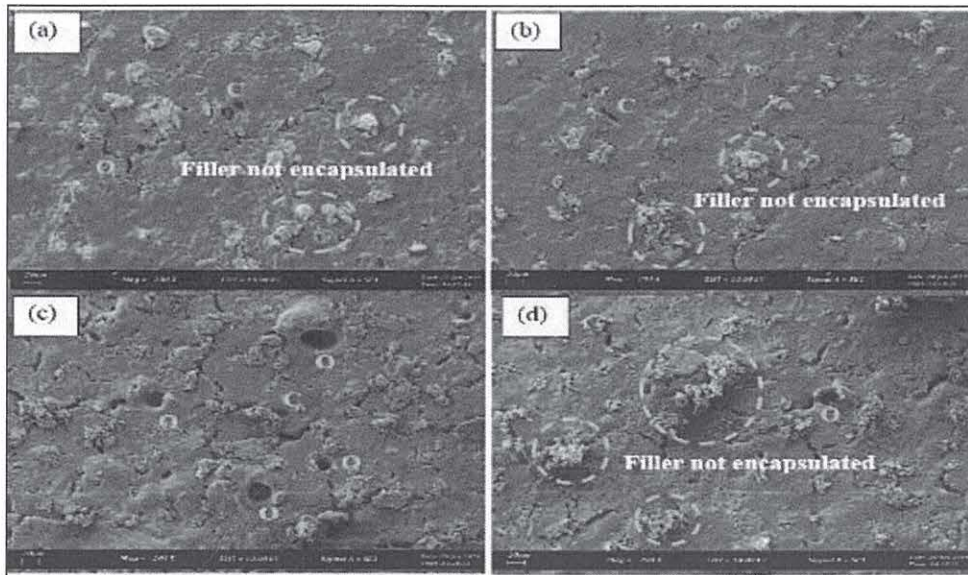


Figure 2.9 SEM micrographs of glass composite sintered at 850°C with varying egg shell contents (a) 5wt.% (b) 10wt.% (c) 15wt.% (d) 20wt.% [Indicator: O – Open pore; C – Closed pore](Mesri et al., 2020b)

The fabrication of Alumino-Silicate-Fluoride (ASF) based bio-glass derived from waste clam shell and soda-lime silica glasses has been studied by Rahman *et al.*, (2019). In this study, the filler loading weight percentage is 5, 10, 15, and 20 wt.%. The samples were sintered at 1500°C for 4 hours. The microstructure of bio-glass samples may be fully examined and analyzed using field emission scanning electron microscopy (FESEM). Microscopic images of glass samples were examined using FESEM analysis, which included grain size, shape, and morphology. According to the FESEM examination, all bio-glass samples displayed uneven particle distribution, irregular shape and varied grain size. The distinction is that the amount of CaO in the composition does not influence the sample's increased crystallinity. All of the glass samples exhibited a clean glass surface with no indication of crystal formation, as illustrated in Figure 2.10 below.

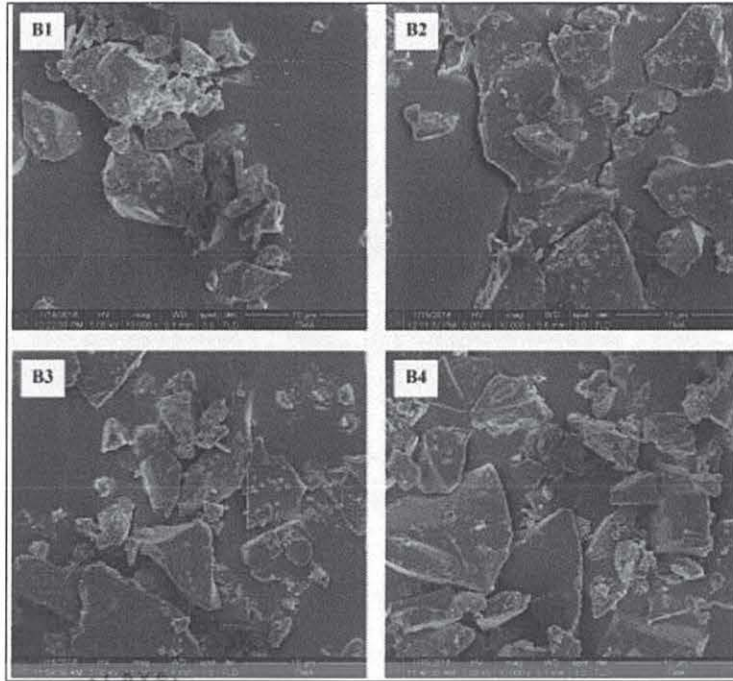


Figure 2. 10: FESEM micrograph of ASF bio-glass samples before sintered at B1:5wt. %, B2:10wt.%, B3:15wt.%, and B4:20wt.% (Rahman et al., 2019)

An investigation by Shamsudin *et al.*, (2019) investigated the physical properties and morphological of sintered cockle shell/recycled soda-lime silicate composite. The formulation of the filler load of cockle shell (CS) is 30wt.%, 40wt.% and 50wt.%. Scanning electron microscopy (SEM) was used to study the apparent morphology of sintered glass composite. Figure 2.11 below illustrated the sintered glass-ceramic composite with 30wt.% of CS filler. Because of the large glass volume, the microstructure of the 30 wt.% cockle shell sample reveals more crystal. This implies that crystallisation occurs at the expense of bulk glass. It also has the fewest pores and the thickest surface.

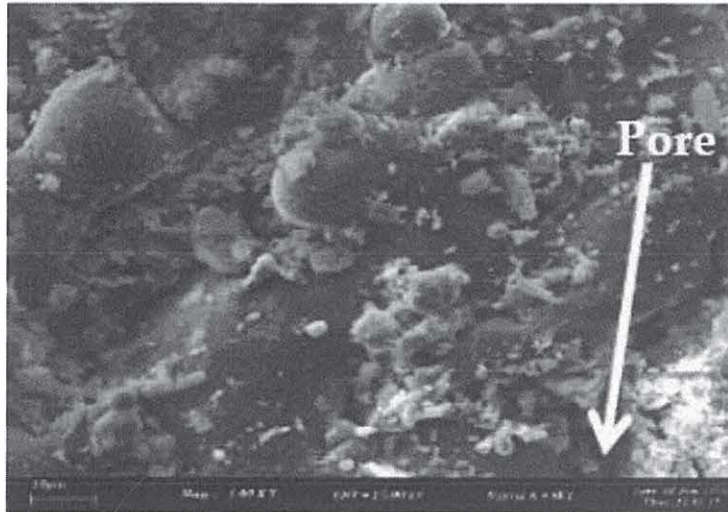


Figure 2. 11: Micrograph of glass-ceramic composite with 30wt.% of CS (Shamsudin et al., 2019)

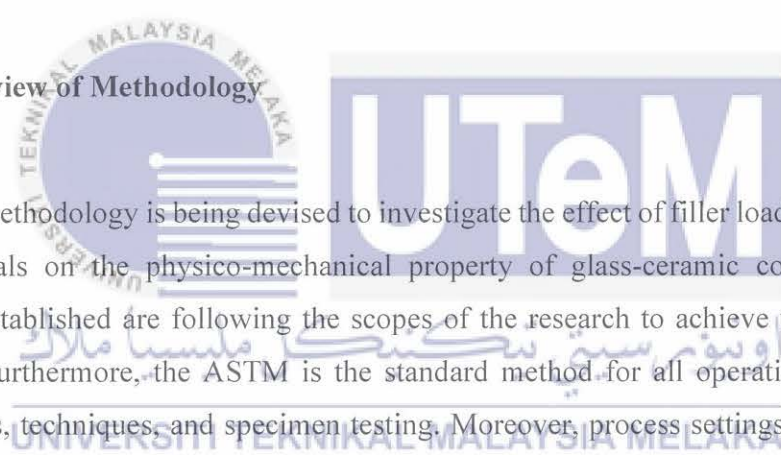


CHAPTER 3

METHODOLOGY

This chapter outlines the suggested approach for this research, which includes the concepts of the procedures that were used to finish the study. Following a thorough analysis of the specification and specifics of prior research, the material selection, processing and testing were provided. The central idea of methodology is to provide appropriate approaches, tools, and methods to conduct this study.

3.1 Overview of Methodology



The methodology is being devised to investigate the effect of filler loading from eco-waste materials on the physico-mechanical property of glass-ceramic composite. The procedures established are following the scopes of the research to achieve the objectives mentioned. Furthermore, the ASTM is the standard method for all operations including standard tools, techniques, and specimen testing. Moreover, process settings are based on previous research. The flow chart is shown in Figure 3.1 below outlines the overall process of obtaining the final result, which includes, material and sample preparation, fabrication of the sample, testing methods, and data analysis.

3.1.1 The Relation between Objectives and Methodology

The significance of the method employed to accomplish the objectives is illustrated in Table 3.1. To meet the quality standards for this study, the appropriate procedures for each of the aims were applied.

Table 3. 1: The significance of methodology used in the study

Objective	Method
<p>1) To characterise the effect filler loading (wt.%) of the cockle shells (CS) in the physical properties in the recycled soda-lime silicate (SLS) glass at different sintering temperatures.</p>	<p>Forming Process:</p> <ul style="list-style-type: none"> • Machine: Manual Hydraulic Press • Mould Dimension: 18 mm x 18 mm x 4 mm • 10 tonnes <p>Sintering Process:</p> <ul style="list-style-type: none"> • Laboratory Electric Furnace: Carbolite 1300 <p>Physical Test:</p> <ul style="list-style-type: none"> • ASTM C373 <p>Characterization of Material:</p> <ul style="list-style-type: none"> • Fourier Transform Infrared Spectroscopy (FTIR) <p>Phase Identification:</p> <ul style="list-style-type: none"> • PANalytical X-ray Diffraction (XRD): X'Pert Pro MPD PW3060/60
<p>2) To measure the mechanical properties of SLSG/CS glass-ceramic composite using microhardness testing and acoustic method.</p>	<p>Microhardness Test</p> <ul style="list-style-type: none"> • Vickers Hardness Test • ASTM C1327-99 <p>Ultrasonic Test:</p> <ul style="list-style-type: none"> • Ultrasonic Pulse Velocity • ASTM E494-95
<p>3) To correlate the effect of filler loading on physico-mechanical to morphology from the literature review.</p>	<p>Microstructure Observation:</p> <ul style="list-style-type: none"> • Literature review

3.1.2 Flow Chart for Process Planning

The flow chart is used to build the planning process. The flowchart of the planning process is detailed to help the reader understand how the technique is used and moved. This study's flow chart is depicted in Figure 3.1.

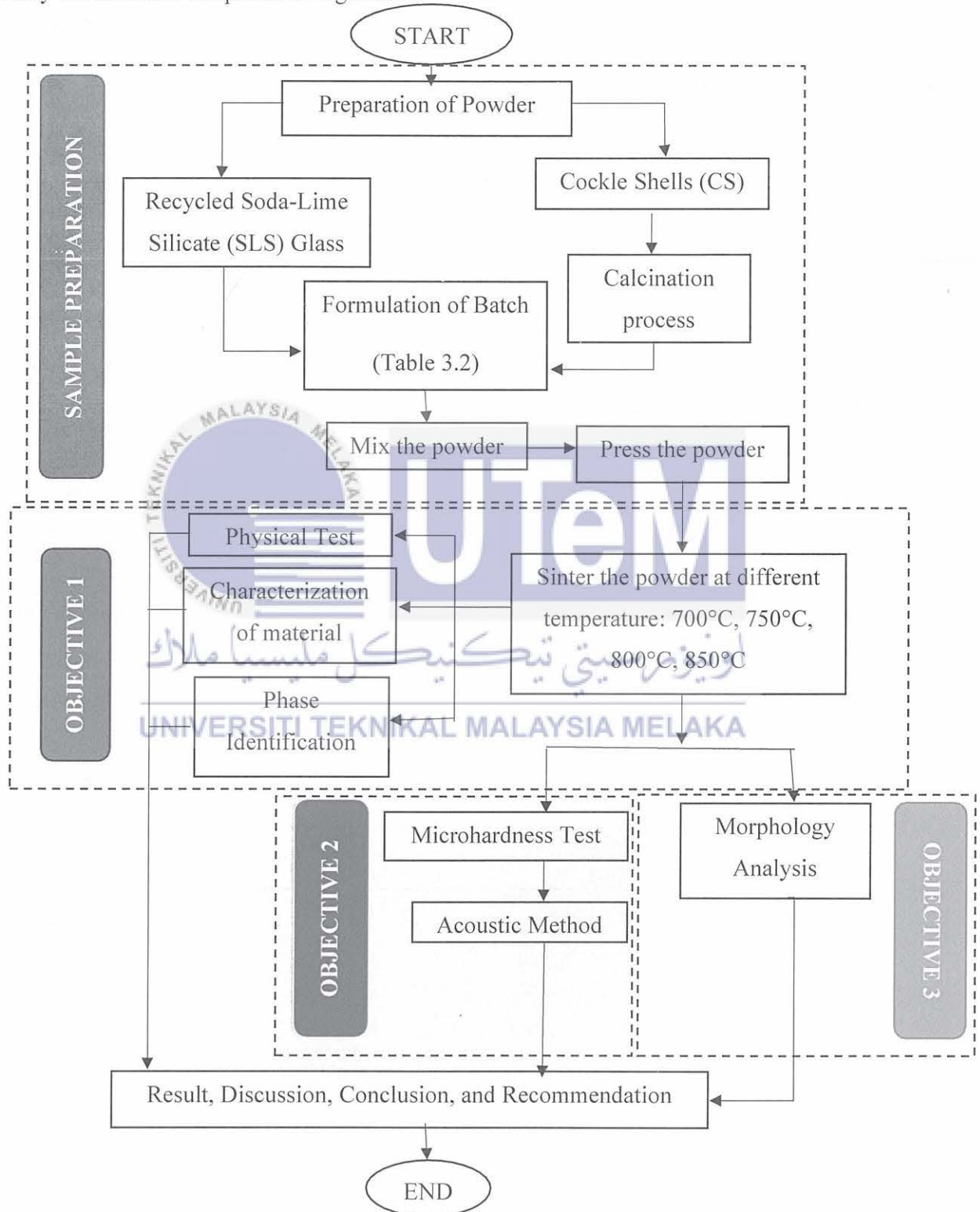


Figure 3. 1: The Flow Chart for Process Planning

3.2 Preparation of Powder

The preparation of powder is divided by the materials which are recycled soda-lime silicate (SLS) glass and cockle shells (CS). This is because the preparations for both of the materials are different. The preparations are explained in the subtopic below.

3.2.1 Recycled Soda Lime Silicate Glass (SLSG)

Recycled soda lime silicate glass (SLSG) is from glass bottle waste. It was obtained from household wastes; the glass bottle must be clear. Figure 3.2 illustrates the clear glass bottles from household waste. Then, it was cleaned and dried under the sunlight for one day. Next, the glass bottle was manually crushed using a pile of cloth and a hammer. Figure 3.3 displays the crushed glass using a hammer. The glass bottle that had been crushed was layered under the pile of cloth to avoid the shards. The coarse particle of the glass bottle that had been obtained was put inside the planetary ball mill (INSMART) as displayed in Figure 3.4 to achieve a fine particle. Then, sieved with a vibratory sieve shaker (OCTAGON Digital) with a 75 μm of stainless-steel sifter to obtain an average particle size of 75 μm . The vibratory sieve shaker and 75 μm sifter are depicted in Figure 3.5 and Figure 3.6. The GCC requires fine powder since particle size affects the ultimate result of the GCC. Then, the finished glass powder was stored in a suitable container at room temperature and convenient to retrieve if desired.

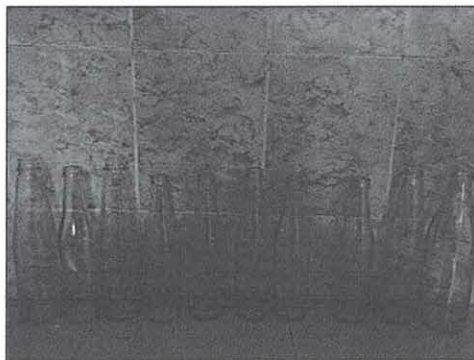


Figure 3. 2: Clear glass bottle from household waste

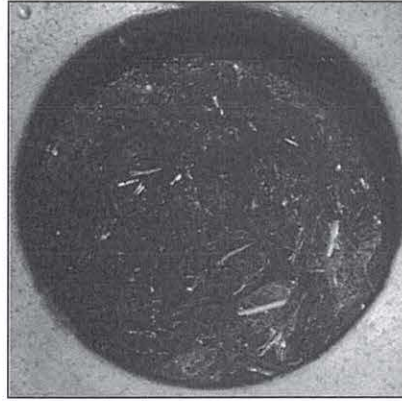


Figure 3. 3: Size of crushed SLSG using a hammer

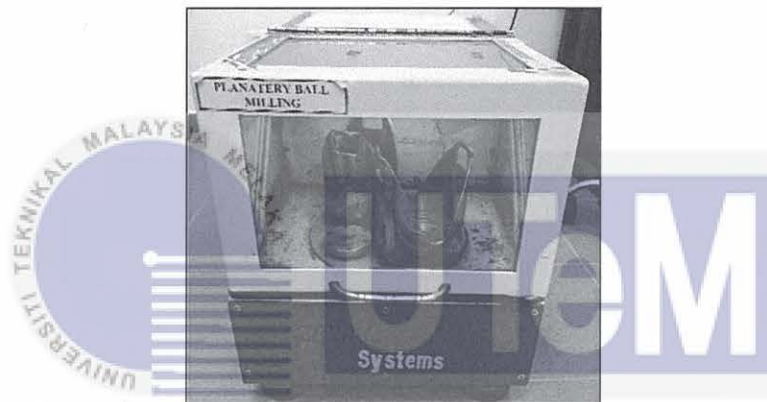


Figure 3. 4: Planetary Ball Mill used to crush the coarse particle into a fine particle

UNIVERSITI TEKNIKAL MALAYSIA MELAKA



Figure 3. 5: Vibratory sieve shaker



Figure 3. 6: Size of 75 μ m of stainless-steel sifter

3.2.2 Cockle Shell (CS)

Figure 3.7 depicts the cockle shell wastes that were obtained from the cockles that have been bought from the market. The cockle shells (CS) were purified to remove dirt and contaminants. Then, CS was dried under sunlight for two days. The shells were crushed into small pieces using pestle and mortar then the pieces were pulverized as demonstrated in Figure 3.8. Next, the powdered shell is sieved using a siever shaker (OCTAGON Digital) to achieve the appropriate particle size, which was approximately 75 μ m. Then, one crucible container, as shown in Figure 3.9, containing powdered cockle shell is calcined at 1000 $^{\circ}$ C temperature with a heating rate of 10 $^{\circ}$ C/min for four hours (Shamsudin et al., 2019). Before usage, the calcined powder is maintained in a tightly sealed container containing silica gel to avoid reactions with carbon dioxide and humidity.



Figure 3. 7: Cockle shell waste

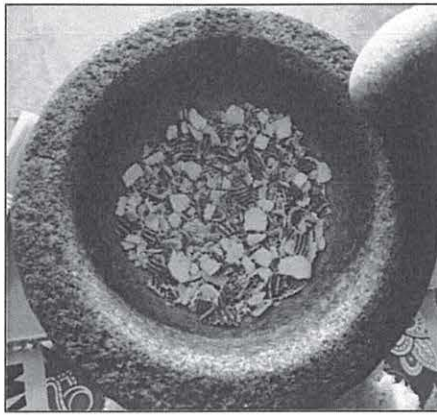


Figure 3. 8: CS in pestle and mortar

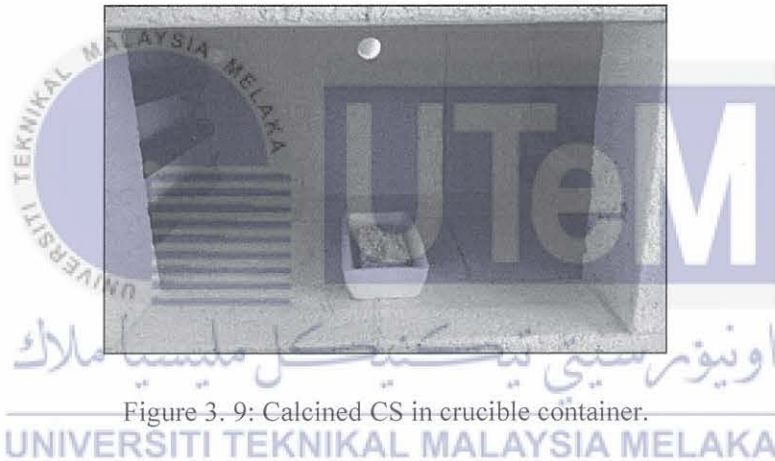


Figure 3. 9: Calcined CS in crucible container.

3.3 Formulation of Batch

In this study, there were a total number of four batches. The batches were divided according to the formulation of the filler loading (wt.%). The code used to identify the batches is A, B, and C. For batch A, the composition is 70wt.% recycled SLS glass and 30wt.% of CS. Whereas for batch B, it has 60wt.% of recycled SLS glass and 40wt.% of CS, batch C has 50wt.% of recycled SLS glass and 50wt.% of CS. The formulation of the batch is obtained from a study by Khemthong *et al.*, (2012a). The formulation of the batch in this study is shown in Table 3.2 below.

Table 3. 2: Formulation of batch (Khemthong et al., 2012b)

Code	Formulation (wt.%)	
	SLSG	Cockle Shells (CS)
A	70	30
B	60	40
C	50	50

3.4 Mixing of Batch

Before the forming process, the powders were mixed together to ensure the materials were spread uniformly. Weighing paper was used to weigh both of the powders on weighing scale according to the formulations of the GCC in Table 3.2. A planetary ball mill was used to combine the SLSG and CS powders. The batches of glass composite were weighed with an accuracy of $\pm 0.01\text{g}$ to 0.05g using a weighing scale. The powder was put into two stainless-steel bowls with five stainless-steel balls on each bowl for 20 minutes. After the powder has been mixed, it was stored inside an airtight container with silica gel to avoid carbon dioxide and humidity.

UNIVERSITI TEKNIKAL MALAYSIA MELAKA

3.5 Processing recycled soda-lime silica (SLS) glass and cockle shells (CS) composite

All of the samples for the recycled SLS glass and CS composite are created by utilising conventional powder processing procedures such as pressing and sintering. The recycled SLS glass powder and CS powder are formed together using uniaxial dry pressing.

3.5.1 Forming Process

The uniform distribution of the batch's formulation was moulded into a square shape with dimensions of 18mm x 18mm x 4mm. As depicted in Figure 3.10, the samples were

produced by uniaxial pressing. By exerting pressure in a single axial direction using a hard punch, the powder mixture was pressed into the rigid die. The applied pressure was 10 tonnes, and the pressed samples were maintained in the rigid die for about a minute before the rigid die punch was released. The square type green pieces were produced using a rigid die with dimensions of 18mm x 18mm x 4mm. A pressure of 10 tonnes was applied to construct a compact element over the combined powders, which will increase the green strength and result in a good consolidated powder. Prior to compacting, the mass of the formulations was measured using a weighing scale with an accuracy of 0.01g to 0.05g. The total number of specimens required for all tests was 32 square-shaped samples for both physical and mechanical testing. Before commencing the sintering process, a picture of the prepared samples was acquired to compare with the image captured after the sintering process. Each sample's colour changes were observed and documented.

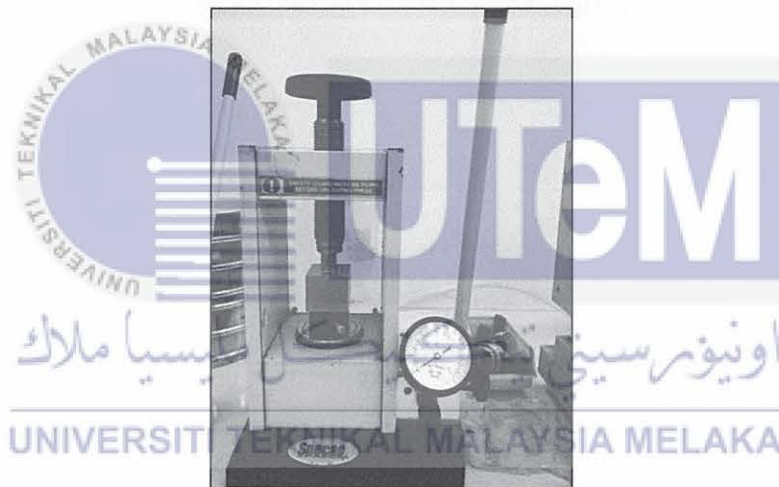


Figure 3. 10: Uniaxial Pressing

3.4.2 Process of Sintering Temperature

After the recycled SLS glass's powder and CS's powder has been pressed, the powder will be sintered at different sintering temperature which are 700°C, 750°C, 800°C, and 850°C with the constant heating rate at 2°C/min and with a constant dwelling time 60 minutes. The powder will be sintered using a laboratory electric furnace (Carbolite 1300). A study by(Gualberto et al., 2019) divided the powder according to temperature respectively. Table 3.3 displays that the samples are divided according to the formulation of

the filler loading (wt.%) and sintering temperature. The table also displays the heating rate, sintering temperature and dwelling time. Firstly, the first batch of the sample is put inside the laboratory electric furnace and will be heated at the first sintering temperature at 700°C as demonstrated in Figure 3.11. The samples will be stored inside an airtight container after the samples were cooled. The sintering process was carried out at the University Teknikal Malaysia Melaka's (UTeM) Centralized Furnace/oven Laboratory. Figure 3.12 illustrates the single step sintering technique employed in this investigation to sinter the samples. Then, elemental analysis, physical test, phase identification, microstructure observation, and mechanical properties analysis are performed on all of the samples.

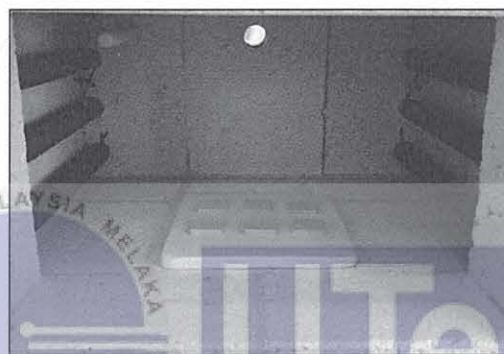


Figure 3. 11: Samples in Electric Furnace

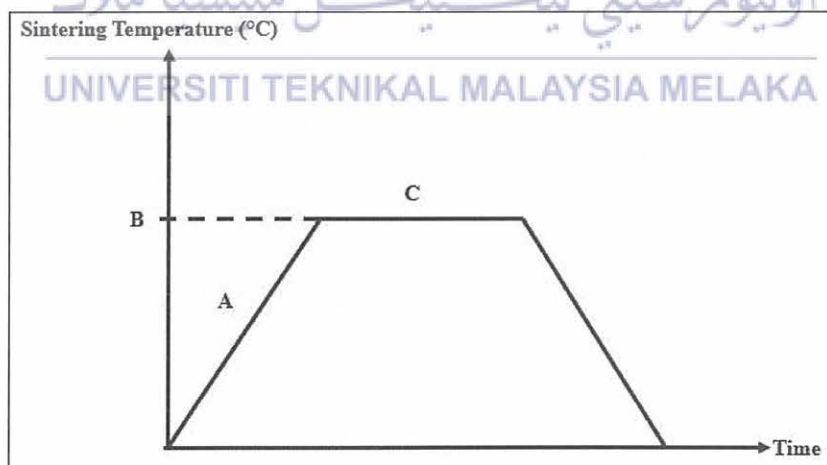


Figure 3. 12: Sintering profile's schematic diagram

Table 3. 3: Parameters for Sintering Process

Batch	Code	Formulation of batch (wt.%)	Material	B: Sintering Temperature (°C)	A: Heating Rate (°C/min)	C: Dwelling Time (min)
Batch 1	A1	100	SLSG	700°C	2°C/min	60 minutes
	A2	70:30	SLSG:CS			
	A3	60:40				
	A4	50:50				
Batch 2	B1	100	SLSG	750°C		
	B2	70:30	SLSG:CS			
	B3	60:40				
	B4	50:50				
Batch 3	C1	100	SLSG	800°C		
	C2	70:30	SLSG:CS			
	C3	60:40				
	C4	50:50				
Batch 4	D1	100	SLSG	850°C		
	D2	70:30	SLSG:CS			
	D3	60:40				
	D4	50:50				

3.5 Characterization of CS powder

The process of measuring and determining the physical, chemical, mechanical, and microstructural properties of materials is known as material characterisation. Characterization of raw materials is critical in the quality control process of product manufacture or development, ensuring that impurities, residual solvents, catalysts, water, particles, and/or degradants meet standards. In this study, the element of calcined CS powder was analysed using Fourier Transform Infrared Spectroscopy (FTIR). After CS

powder has been calcined, 1.8g of the powder was taken for FTIR analysis. The analysis was conducted in Nano-materials Laboratory, UTeM. Then,

3.6 Characterization of GCC

3.6.1 Apparent Porosity, Bulk Density, and Linear Shrinkage

The apparent porosity is the physical analysis of the recycled SLS glass and CS composite, and it can be determined using the ASTM C373 standard. The apparent porosity, %AP, expresses the correlation between the volume of the specimen's open pores and its outer volume as a percentage. The equation to calculate the porosity is as the Equation 3.1 below, where %AP is the apparent porosity, V is the exterior volume in a cubic centimetre, D is the dry mass in gram, and M is the saturated mass in gram.

Berger (2010) used Archimedes buoyancy technique with dry weights, soaked weights and immersed weights in water to calculate the apparent porosity (%AP). According to the Archimedes Principle, the buoyant force on a submerged object is equal to the weight of the fluid displaced by the object. The sample for each different sintering temperature and different filler loading is selected. The dry mass, D is determined to the nearest 0.01 g. M is the saturated mass of the sample and V is the volume of sample in cm³. The samples are placed in a pan of distilled water, ensuring the samples are covered with water. Setter pins or a similar device can be used to separate the specimens from the bottom and sides of the pan, as well as from one other. Equation 3.2 was used to calculate the bulk density. The result of the bulk density was compared with the experimental value of the sample using densimeter, where ρ is the bulk density, W_a is weight of the sample in air, W_b is weight of the sample in distilled water, and ρ_b is density of distilled water. Then linear shrinkage, L was calculated using Equation 3.3.

$$\%AP = \left[\frac{M - D}{V} \right] \times 100 \quad \text{Equation 3.1}$$

$$\rho = \frac{W_a}{W_a - W_b} \rho_b \quad \text{Equation 3.2}$$

$$L = \frac{\text{Initial Diameter} - \text{Final Diameter}}{\text{Initial Diameter}} \quad \text{Equation 3.3}$$

3.7 Characterization of sintered recycled SLS glass and CS composite

3.7.1 Identification of phase

The sample of recycled glass SLS glass and CS composite for each different sintering temperature were used for this phase identification. This analysis used wide-angle X-Ray Diffraction (XRD) to distinguish the nature of the samples' amorphous and crystalline components at different sintering temperatures and different filler loading. XRD measurement was investigated with the Cu-K radiation in the 2θ range from 20° to 80° using X'PERT PRO PANalytical software. To determine the crystal phase of foam glass-ceramics, the software X'Pert Highscore plus (PANalytical) was utilised. According to Jusoh et al., (Jusoh et al., 2019a) the crystalline phase will differ based on the sintering temperature. The crystalline phase of the samples that sintered at 700°C , 750°C , 800°C and 850°C were analysed to observe the phase at each temperature. Figure 3.4 depicts a scan of a mixture of crystalline (Ermrich & Opper, 2011).

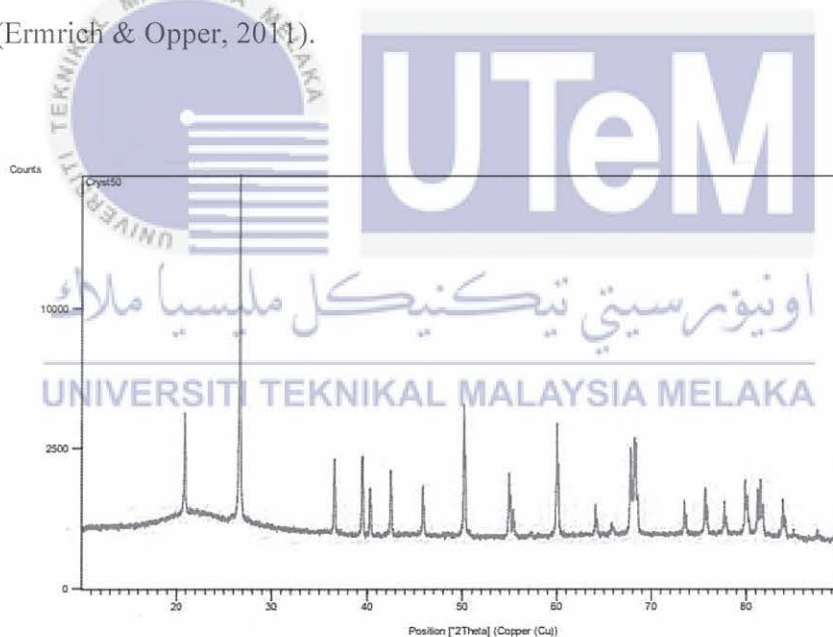


Figure 3. 13: Typical powder pattern (Ermrich & Opper, 2011)

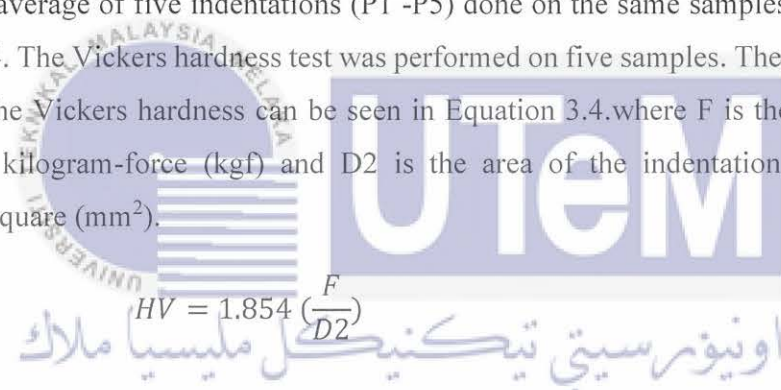
3.8 Mechanical properties analysis

In this study, the mechanical property that had been analysed was the microhardness property of the recycled SLS glass and CS composite. This is due to the potential application

as a building material. Due to unforeseen issues, the samples that have been prepared were tested under microhardness test.

3.8.1 Microhardness Test

The mechanical properties of the GCC samples were investigated using the Vickers hardness test. The GCC's microhardness was determined using an HM-200 Series Microhardness Testing Machine. The surface of the samples should have a consistent and well-polished surface, and the roughness should be less than $0.1\mu\text{m rms}$, according to ASTM-C1327-99: Standard test procedure for Vickers indentation hardness of advanced ceramics. In these tests, the load was 0.5kg for 5 seconds. The hardness measurements were based on the average of five indentations (P1 -P5) done on the same samples as illustrated in Figure 3.14. The Vickers hardness test was performed on five samples. The mathematical solution for the Vickers hardness can be seen in Equation 3.4. where F is the applied load measured in kilogram-force (kgf) and D^2 is the area of the indentation measured in millimetres square (mm^2).



$$HV = 1.854 \left(\frac{F}{D^2} \right) \quad \text{Equation 3. 4}$$

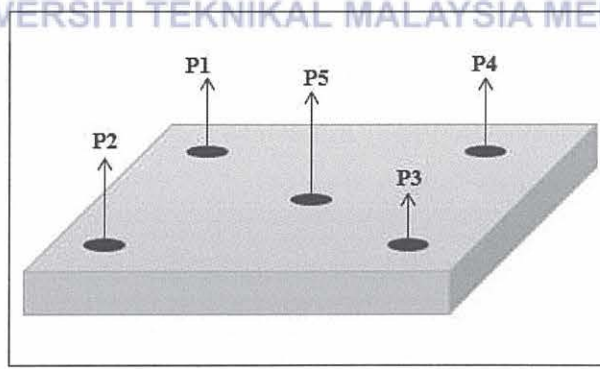


Figure 3. 14: Schematic of five indentations on sample.

3.9 Acoustic Measurement

The propagation and reflection of sound waves through the thickness of a specimen is the basis for ultrasonic velocity measurements. In order to acquire Young's Modulus, this

approach used two types of transducers that produced longitudinal and transverse (shear) waves (Franco et al., 2011).

3.9.1 Ultrasonic Pulse Velocity

Each sample of the recycled SLS glass and CS composite sintered at 700°C, 750°C, 800°C and 850°C with flat parallel surfaces and the thickness of each to an accuracy of ±0.02 mm is measured. Each sample's Young's modulus was calculated by measuring the longitudinal sound wave velocities with an EPOCH 650 series Olympus Ultrasonic Flaw detector, as illustrated in Figures 3.15 and 3.16. The frequency range employed for modulus measurement ranges from 0.1 MHz to 20 MHz, depending on the width of the resonance curve.

The measurements were taken at room temperature. To increase sound wave transmission between the transducer and the samples, samples were pre-smearred with a water-based (Magnaflux) coupling medium. For the computation of Young's modulus, the time-of-flight, or the time it took for a wave to be released by the transducer, reflected by the sample, and received by the transducer, was recorded. The time-of-flight data were obtained as the mean of three measurements.

The search unit for each sample is aligned and a nominal signal pattern of as many back echoes as are clearly defined will be obtained, as shown in Figure 3.15 The longitudinal and transverse wave times-of-flight in each specimen were measured between the second and third back wall echoes. Acoustic measurements have been carried out in accordance with the principles outlined in the test standard ATSM E 494-95. Equation 3.5 was used to calculate the longitudinal velocity, v_l , based on the transit time across the thickness of the samples.

$$v_l = \frac{2 \times d (m)}{t(s)} \quad \text{Equation 3. 5}$$

Where v_l , d , and t represent the longitudinal wave velocity, sample thickness, and time-of-flight, respectively.

The Young's modulus was derived from the aforementioned measurements using Equation 3.6 (Zaid et al., 2011).

$$E = \rho v_l^2$$

Equation 3. 6

where ρ denotes the density of the tested sample and v_l denotes the longitudinal velocity of each sample tested.

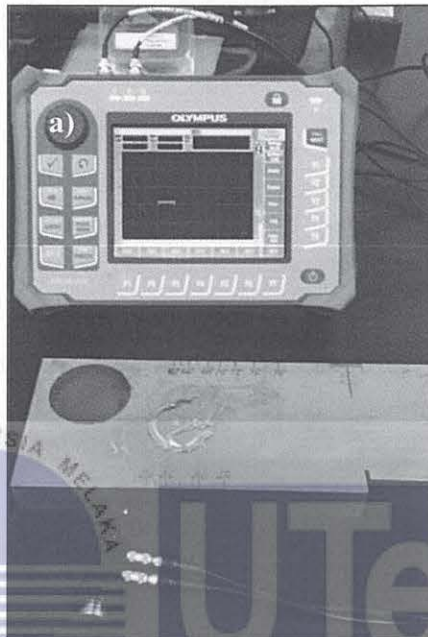


Figure 3. 15: The EPOCH 650 Series Olympus Ultrasonic Flaw Detector

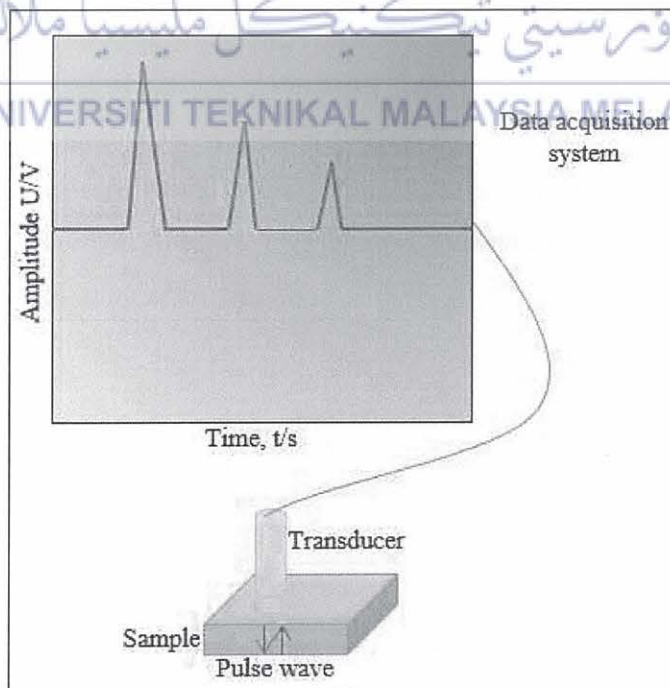


Figure 3. 16: Schematic of Ultrasonic Pulse Velocity Diagram

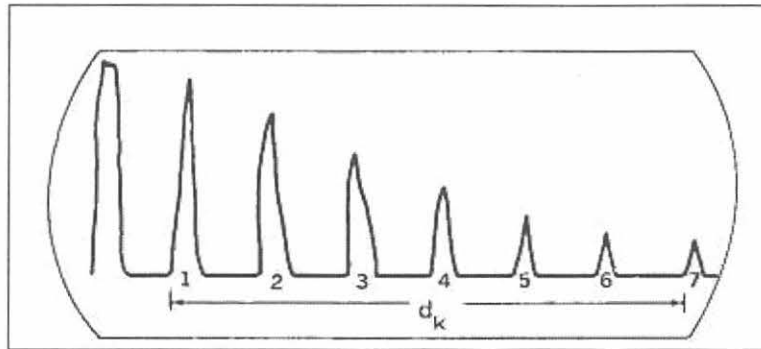


Figure 3. 17: 7 Back Echoes and Initial Pulse (ASTM E494 - 95 Standard Practice for Measuring Ultrasonic Velocity in Materials, *n.d.*)

3.10 Morphology Analysis

3.10.1 Scanning Electron Microscope (SEM)

The microstructure of the sintered sample was observed by scanning electron microscopy (SEM). SEM is an imaging technique that employs electrons. The electrons in the beam interact with the sample, producing a variety of signals that can be utilised to determine the surface topography and composition. SEM (EVO 50 Carl Zeiss SMT) is used to observe the surface of the recycled SLS glass and CS composite sintered at 700°C, 750°C, 800°C, and 850°C with a different filler loading 30 wt.%, 40 wt.% and 50wt.%. It was also used to obtain the characterization images for the distance between the defect and the surface, which was supported by an A-scan display. By using the SC-7620 mini sputter, the surfaces of the samples were coated with gold layers at an adequate size to confirm that the samples are conductive. This is due to their inability to conduct electrons, and SEM requires a conductive surface to work effectively.

CHAPTER 4

RESULT AND DISCUSSION

This chapter comprises the findings and discussion of a study involving the characterisation of raw materials. The raw materials used are powdered soda-lime silicate glass (SLSG) and cockle shell (CS). To support the physical and mechanical characteristics of the glass-ceramic composite after sintered at varied sintering temperatures with constant heating rate and holding duration, microstructure and phase analyses were performed. The physical investigation performed in this study included linear shrinkage, apparent porosity, and bulk density. The mechanical characteristics were then analysed using microhardness tests and acoustic measurements.

4.1 Characterization of CS

FTIR analysis was analysed to determine the hydrogen bond in the CS powder. Figure 4.1 displays the existence of a peak at 3641 cm^{-1} for calcination at 1000°C . This result was in the same agreement (Shamsudin et al., 2019) where there is the presence of formation of OH bonds during water adsorption by CaO.

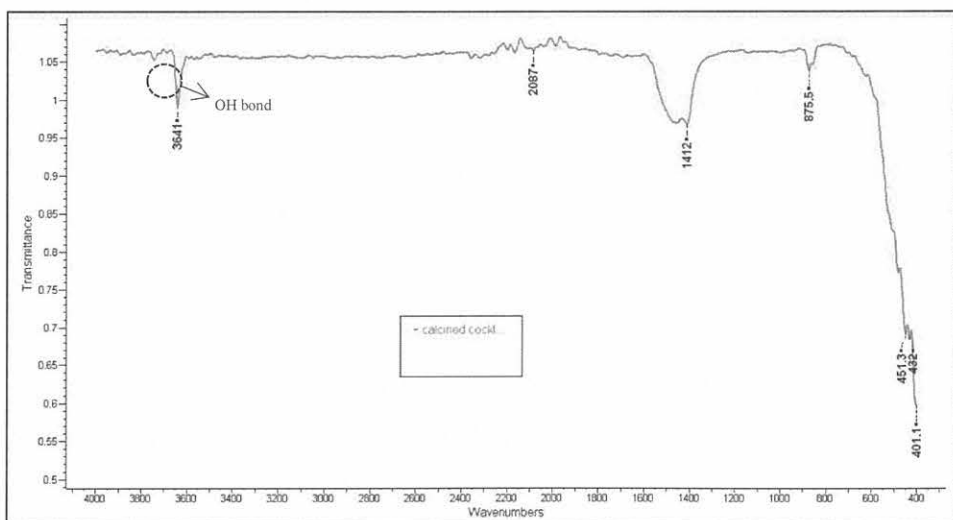


Figure 4. 1: FTIR spectra of calcined CS powder at 1000°C

4.2 The influence of different sintering temperatures on the characteristics of Glass-ceramic composite (GCC)

Physical and mechanical tests were used to investigate the effects of different sintering temperatures on glass-ceramic samples. Visual observations, linear shrinkage, bulk density, and apparent porosity were used to study physical characteristics. Furthermore, phase and microstructural analyses were performed to validate the mechanical characteristics derived from microhardness tests and ultrasonic procedures. Sintered samples of various compositions were sintered for 1 hour at 700, 750, 800, and 850 °C at a heating rate of 2 °C/min.

4.2.1 Physical Properties

Optical observations, linear shrinkage, apparent porosity, and bulk density were used to investigate physical attributes. The tests were carried out in the Physics Laboratory of UTeM.

4.2.1.1 Visual Observation

The major colour variations for distinct formulation samples with different sintering temperatures are shown in Table 4.1 below. Figure 4.2 depicts the sample prior to sintering. The typical colour of the sample before sintering was grey, but a visual check revealed that the sample of the 100wt.% CS formulation was milky white. After the sintering process, the shade of each formulation varies. Most compositions sintered at 700°C turn dark grey and grey in colour. The sample became dark brown when at SLSG 100wt.%. The colour of samples sintered at 750°C changed to light grey for 40wt.% and 50wt.% CS fillers. The colour of the sample with 30wt.% CS fill, on the other hand, becomes dark grey. The colour of samples containing 100wt.% SLSG was dark brown.

Light grey was the most noticeable colour change for samples sintered at 800 and 800°C with CS filler loading of 30, 40, and 50wt.%. samples containing 100wt.% SLSG become grey. Bharatham et al. (2014) discovered that vividly coloured samples had high levels of calcium. As a result, the CS filler load with 50wt.% samples have a brighter colour than others.

Table 4. 1: The colour differs as the sintering temperature changes.

Sintering Temperature, °C	Formulation of Batch, (wt.%)			
	100	70:30	60:40	50:50
700	 Dark Brown	 Dark Grey	 Dark Grey	 Grey
750	 Dark Brown	 Dark Grey	 Light Grey	 Light Grey
800	 Grey	 Light Grey	 Light Grey	 Light Grey
850	 Grey	 Light Grey	 Light Grey	 Light Grey

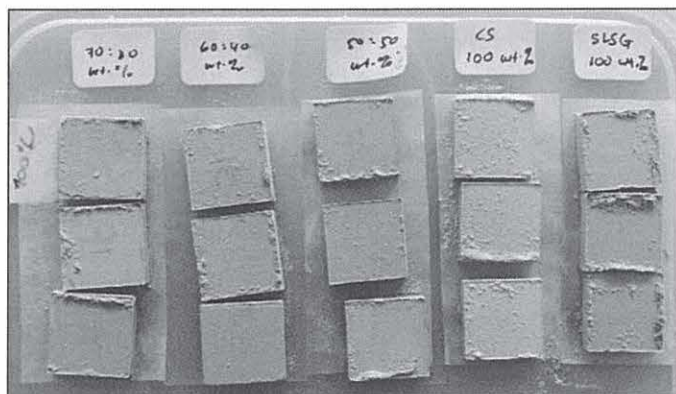

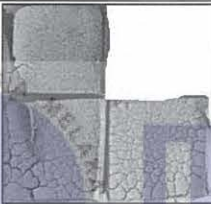


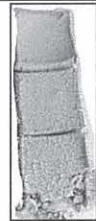


Figure 4. 2: Pressed sample at 5 tonnes before the sintering process

The samples that have been shattered as a result of inappropriate sample handling are shown in Table 4.2 below. It is the end product of two days in an electric furnace. The samples were also expanded and partially shattered. The shattered samples were predicted due to the presence of OH bonds where the SLSG/CS absorbs moisture from the air in the furnace (as illustrated in Figure 4.3) without being stored immediately after sintering within an airtight container containing silica gel. The samples should not be left inside the furnace for a long time.

Table 4. 2: Overdried sample in the furnace

Temperature	700°C				
Formulation, (wt.%)	70:30	60:40	50:50	100 (SLSG)	100 (CS)
Result					

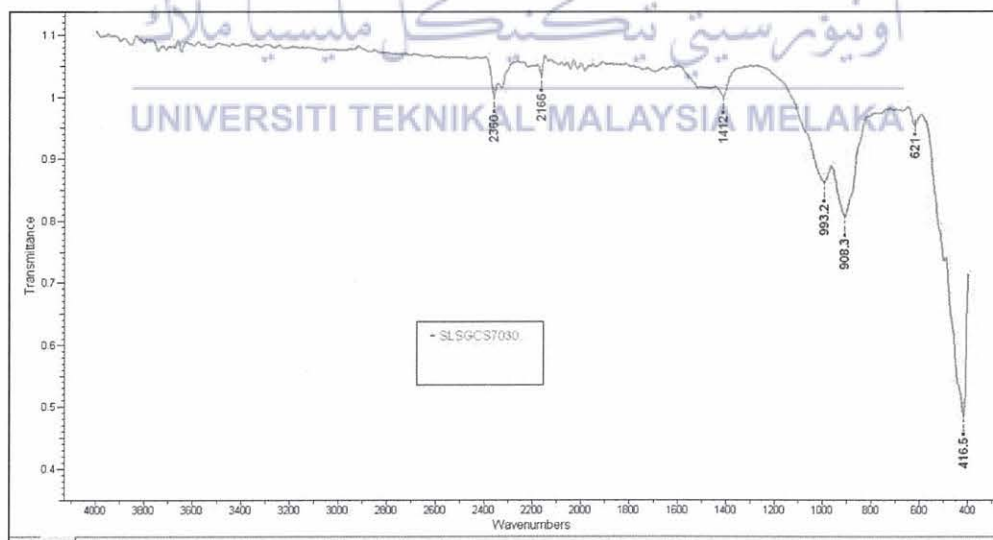


Figure 4. 3:FTIR analysis of the shattered sample

4.2.1.2 Linear Shrinkage

The linear shrinkage of a GCC at different sintering temperatures can be depicted in Figure 4.3 below. The initial sample dimension for all formulations is 18mm x 18mm x 4mm. At 700, 750, 800, and 850°C, the dimension has been shrunk for all formulations containing 100wt.% SLSG with all the value are negative. All samples were sintered at 850°C with 30, 40, and 50wt.% CS filler load, on the other hand, exhibit an expansion in dimension. The maximum expansion of the sample is at 750°C with 30wt.% of CS filler load, 10.56cm. This is due to the crystallization and the densification that occur during the crystallization temperature, T_c , 750°C (Salleh et al., 2017).

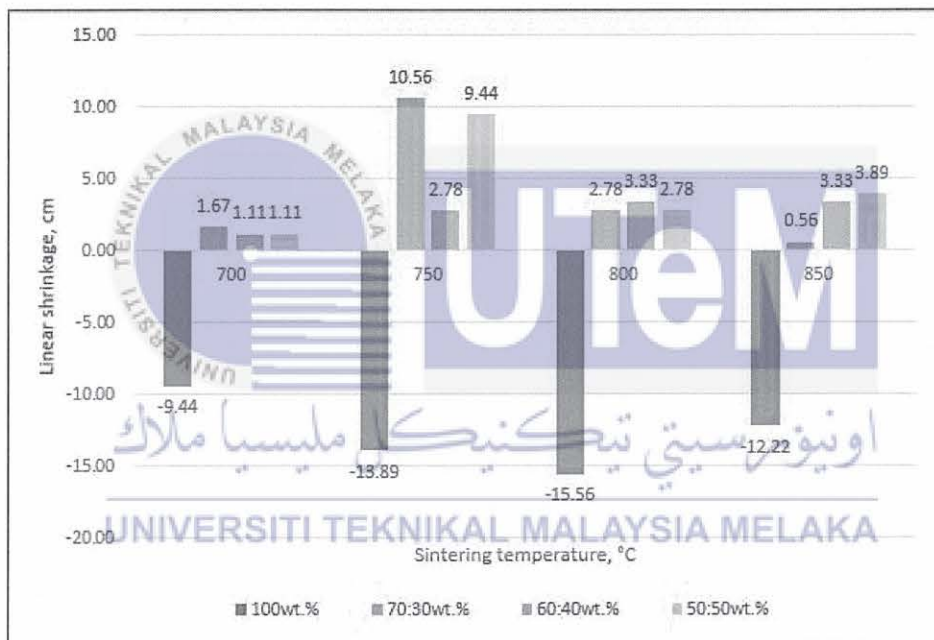


Figure 4. 4: GCC's linear shrinkage at different sintering temperature

Table 4. 3: Data for linear shrinkage of GCC at different sintering temperature

Sintering Temperature (°C)	Formulation of GCC			
	100	70:30	60:40	50:50
700	-9.44	1.67	1.11	1.11
750	-13.89	10.56	2.78	9.44
800	-15.56	2.78	3.33	2.78
850	-12.22	0.56	3.33	3.89

4.2.1.2 Bulk Density

The bulk density for every sample formulation at different sintering temperatures is depicted in Figure 4.5 below. From Figure 4.5 below, the graph of the result for the bulk density shows an inconsistent trend due to the distribution of particle inside the composite. For samples sintered at 850°C show an increasing trend for 30, 40, and 50wt.% of CS filler loading. The samples with 50wt.% of CS filler loading shows a linear relationship between the bulk density and the apparent porosity. When the density is increased, the apparent porosity of the samples with 50wt.% of CS filler loading, increased. But the results can be inaccurate due to the handling of the samples while using densimeter.

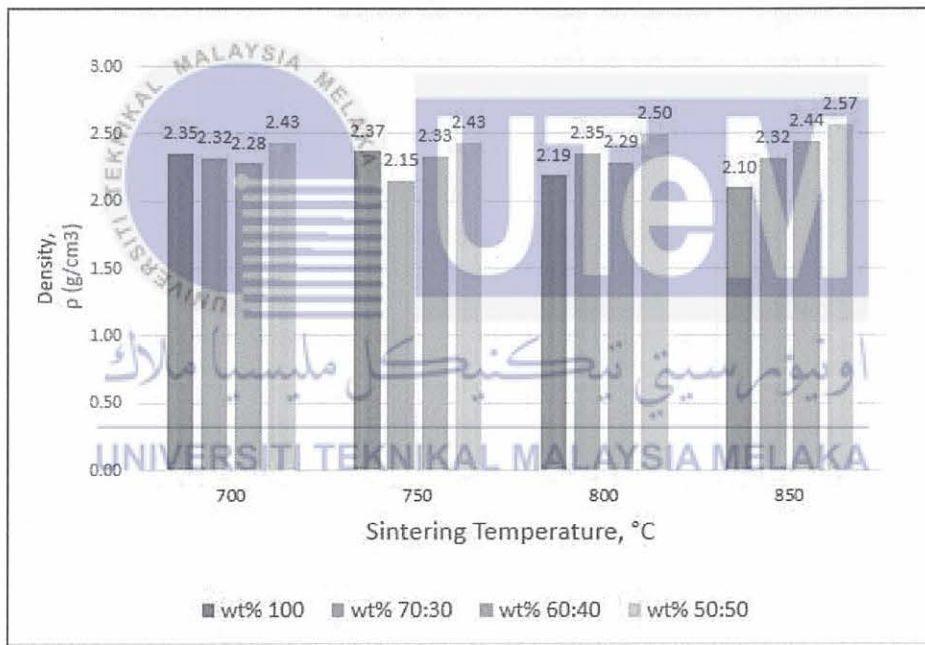


Figure 4. 5: The bulk density for every sample formulation at different sintering temperatures

4.2.1.3 Apparent Porosity

The result of apparent porosity determined using Equation 3.1 is then plotted into the graph displayed in Figure 4.6. The volume of the closed pores is not included in the apparent porosity. According to Figure 4.5, the majority of the samples sintered at 850°C have a higher percentage of porosity than the samples sintered at 700°C. The porosity developed

on each of the samples impacted the varying percentages of perceived porosity. Because of the reduced amount of porosity, the samples with 30wt.% CS filler load had the lowest percentage of porosity at 850°C than the samples at 800°C. Because the cockle shell does not completely fuse with the SLSG, porosity forms in the sample.

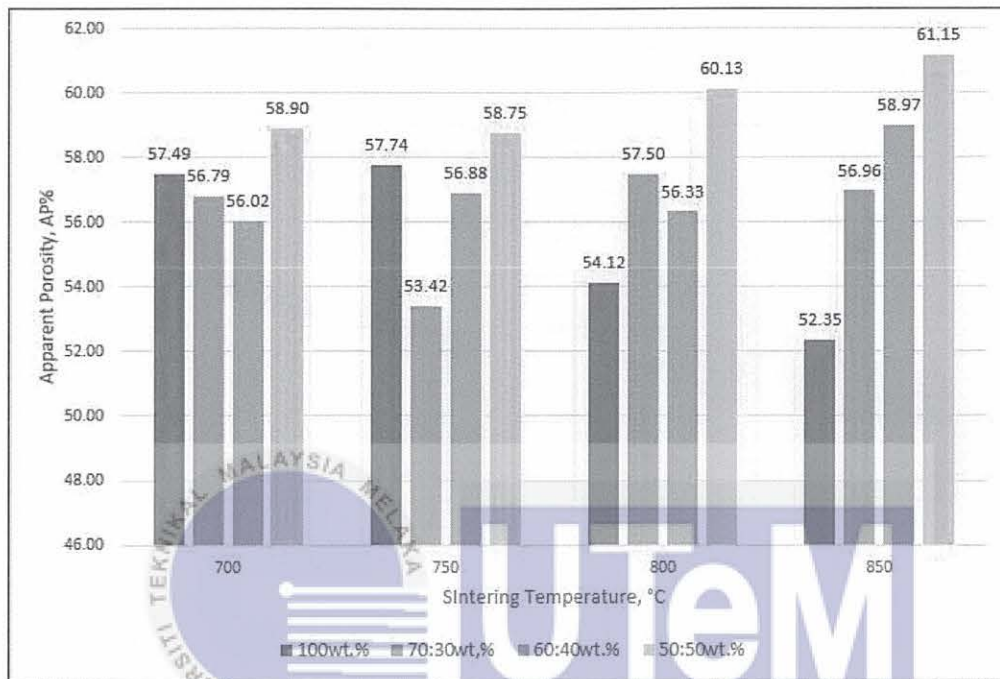


Figure 4. 6: Apparent porosity at different sintering temperature

4.2.2 Phase and Microstructure

4.2.2.1 X-Ray Diffraction (XRD) Analysis

The crystalline phase detected by the GCC's XRD pattern is shown in Figure 4.7. The research demonstrates the formulation of phase transitions as a function of sintering temperature. The primary crystalline found at 850°C sintering temperature with 30wt% CS filler load is quartz and cristobalite. In the XRD patterns, a modest number of crystalline peaks were found, with the peak of quartz located at 2θ 31.891°. These findings suggest that the amount of SLSG in glass composite may have a significant impact on the crystalline phase product, quartz, in the tested formulations of filler load. As a result, the proper sintering temperature of 850°C is critical for obtaining a good glass composite with great

mechanical strength. In addition, there are more peaks for sintering temperature 850°C than other sintering temperature. The sample with 100wt.% SLSG sintered at 750°C reveals that the crystallisation peak does not present in the XRD pattern due to the very amorphous structure. As a result, when compared to samples sintered at 850°C, properties including apparent porosity and bulk density perform poorly.

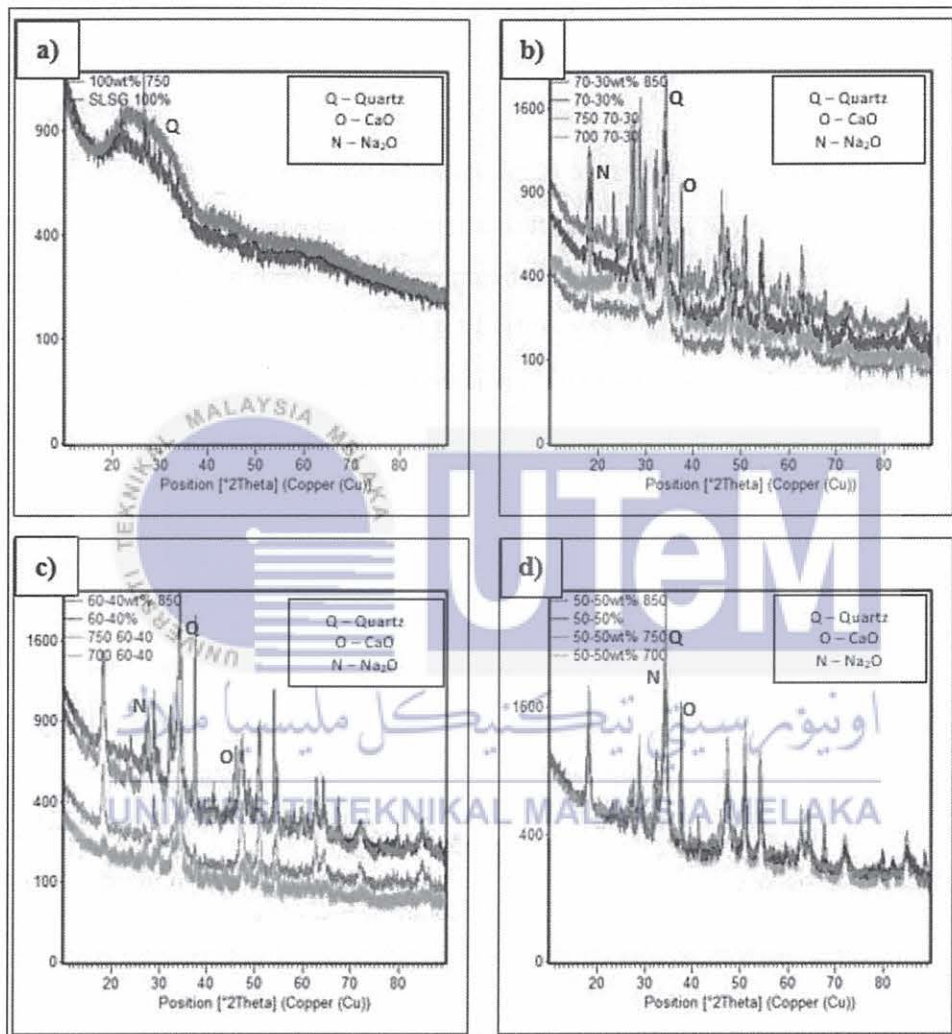


Figure 4. 7: XRD Analysis of the samples at a) 0wt.%, b) 30wt.% c) 40wt.% and d) 50wt.% of CS filler load

4.2.3 Mechanical Property

The ASTM C 1327-99 standard test procedure for samples that were free of flaws (shattered and distortion) to the naked eyes were chosen to evaluate the hardness. Vickers indentation hardness of advanced ceramics was used for the microhardness testing.

4.2.3.1 Microhardness

Table 4.4 displays the results of the microhardness tests. The results show that the sample with 30% CS filler load has the highest microhardness value at 850°C, which is 1004.86Hv. When samples sintered at 700°C were compared to those sintered at 613.58Hv, the hardness increased by almost 38% ($613.58 / (613.58 + 1004.86)$). The formulation of filler load of 30wt.% CS contributed to outstanding mechanical qualities, demonstrating the formulation's superior physical capabilities.

The highest microhardness attained as a result of crystal precipitation in glass. According to Leenakul et al., (2016)'s research, crystal precipitation in glass increases the overall density of the glass composite. As the sintering temperature rises, the average reading result is predicted to rise. The process of indentation is responsible for the decreased average reading. The newly formed indentation may fall right upon a big pore. Furthermore, one of the elements that influenced the microhardness measurement was the cleanliness of the indenter. Aside from that, the surface of the sample should be ground and smooth to maximise the accuracy of the reading.

As indicated in Figure 4.7, the XRD analysis of the samples that sintered with 30wt.% shows that there is more crystalline peak than other formulation of the filler load. The phase existing in the structure influences microhardness; the more crystalline phase present, the greater the microhardness result of the samples may be produced. Furthermore, the decreased hardness of the sample is owing to the presence of micropores and a less crystalline phase. The samples with 30wt.% of CS filler loading has a lower apparent porosity than other formulation of the CS filler load. The intensity of the X-ray lines illustrates how the glassy phase decreases as the sintering process temperature rises.

Table 4. 4: Average reading of microhardness of selected sample.

Sintering Temperature, °C	Formulation of GCC, wt. %	Average Reading, Hv
700	100	477.90
	70:30	249.76
750	100	508.10
850	100	613.58
	70:30	1004.86

4.2.4 Acoustic Measurement

4.2.4.1 Ultrasonic Pulse Velocity

Table 4.5 below depicts the result of the Young's modulus of the selected samples which were free from flaws at different sintering temperature. The Young's modulus was calculated using Equation 3.6. Young's modulus is defined as density multiply with squared longitudinal velocity. The value of E reflects how much strain a glass sample can sustain when subjected to a specific level of stress. From the Table 4.5 below, glass-ceramic composite samples have a Young's modulus of less than 100 GPa. As a result, the lower value of Young's modulus suggested that the glass samples did not tolerate the strain well (Zaid et al., 2011). At 850°C of sintering temperature, Young's modulus for the samples with 30wt.% of CS filler load is 80.74MPa. The modulus for temperature 850°C is lower than the modulus at temperature of 700°C with 100wt.% SLSG. The modulus is reduced due to the addition of 30wt.% of CS filler load as a result of the presence of porosity.

Table 4. 5: Young's Modulus at different sintering temperature

Sintering Temperature (°C)	Formulation of GCC, (wt.%)	Young Modulus, E (Pa)
700	100	83.88 MPa
	70:30	80.74 MPa
750	100	82.83 MPa
850	100	73.04 MPa
	70:30	80.74 MPa

4.3 Surface Morphology Analysis

Due to unforeseen issue during the project, surface morphology analysis cannot be done for the samples. Hence, the comparison of the result for surface morphology analysis were conducted using selected micrograph from previous research. According to Mesri *et al.*, (2020b) the microstructure of the sintered glass composite significantly shifted with variations in eggshell (ES) waste filler loading at different sintering temperatures. As demonstrated in Figure 4.7 and Figure 4.8, with 10wt.% ES loading, fewer pores and a dense surface were found as compared to 5wt.% ES filler. As the sintering temperature increased, at 20wt.% of ES filler, fewer pores were found.

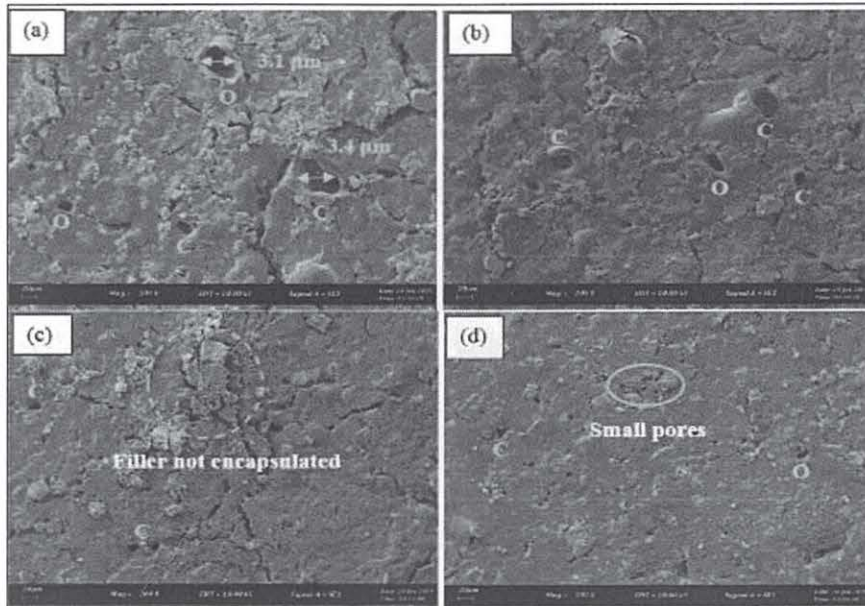


Figure 4. 8: SEM micrographs of glass composite sintered at 800°C with varying egg shell contents (a) 5wt.% (b) 10wt.% (c) 15wt.% (d) 20wt.% [Indicator: O – Open pore; C – Closed pore](Mesri et al., 2020b)

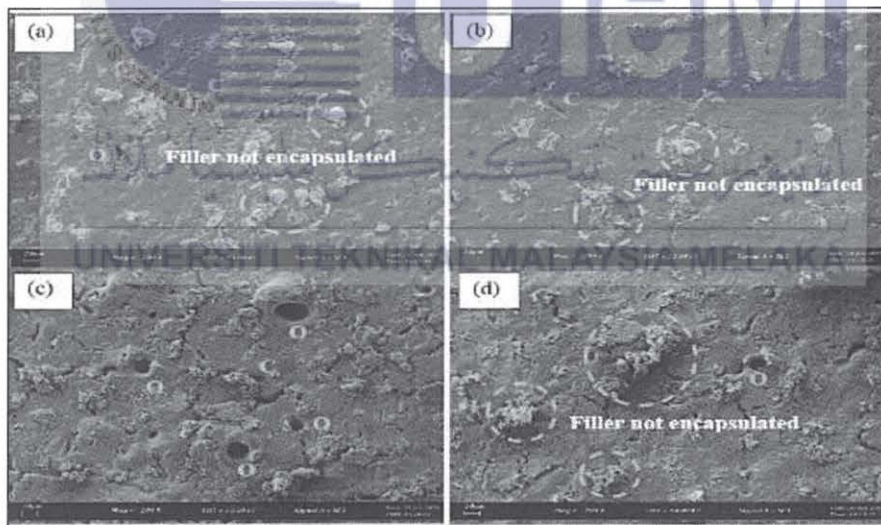


Figure 4. 9: SEM micrographs of glass composite sintered at 850°C with varying egg shell contents (a) 5wt.% (b) 10wt.% (c) 15wt.% (d) 20wt.% [Indicator: O – Open pore; C – Closed pore](Mesri et al., 2020b)

Rahman *et al.*, (2019) investigated the fabrication of Alumino-Silicate-Fluoride (ASF) based bio-glass derived from waste clam shell and soda-lime silica glasses. In this study, the filler loading weight percentage is 5, 10, 15, and 20 wt.%. The samples were sintered at 1500°C for 4 hours. FESEM analysis was used to study microscopic images of

glass samples, which comprised grain size, shape, and morphology. According to the FESEM examination, all bio-glass samples displayed uneven particle distribution, irregular shape and varied grain size. The distinction is that the amount of CaO in the composition does not influence the sample's increased crystallinity. All of the glass samples exhibited a clean glass surface with no indication of crystal formation, as illustrated in Figure 4.9 below.

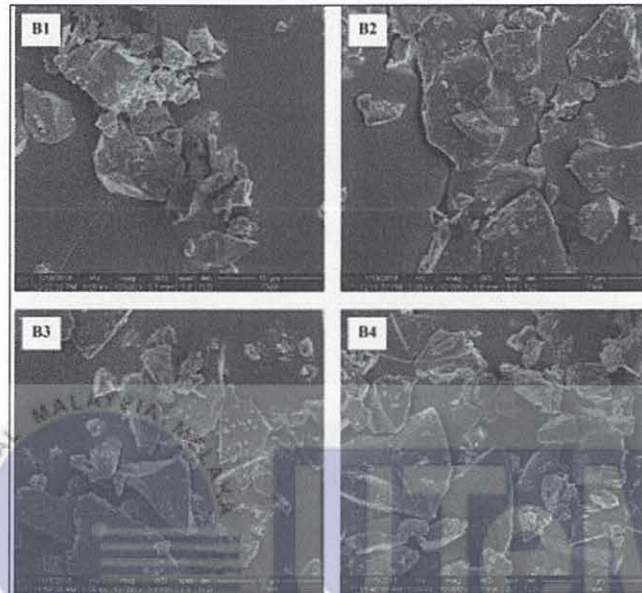


Figure 4. 10: FESEM micrograph of ASF bio-glass samples before sintered at B1:5wt. %, B2:10wt.%, B3:15wt.%, and B4:20wt.% (Rahman et al., 2019)

An investigation by Shamsudin *et al.*, (2019) investigated the physical properties and morphological of sintered cockle shell/recycled soda-lime silicate composite. The formulation of the filler load of cockle shell (CS) is 30wt.%, 40wt.% and 50wt.%. Figure 4.10 below illustrated the sintered glass-ceramic composite with 30wt.% of CS filler. Because of the large glass volume, the microstructure of the 30 wt.% cockle shell sample reveals more crystal. This implies that crystallisation occurs at the expense of bulk glass. It also has the fewest pores and the thickest surface.

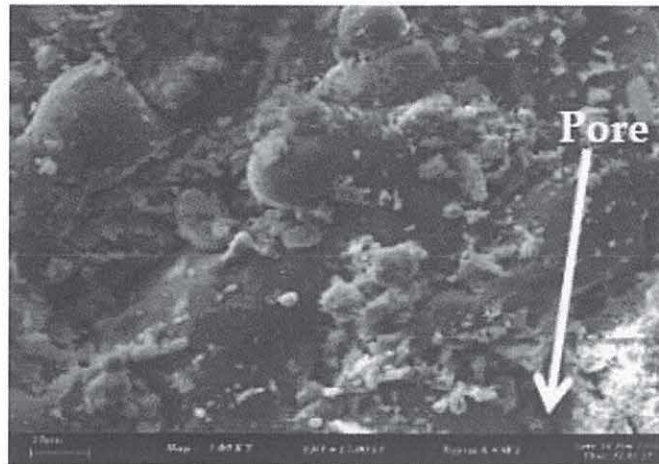


Figure 4. 11: Micrograph of glass-ceramic composite with 30wt.% of CS (Shamsudin et al., 2019)



CHAPTER 5

CONCLUSION & RECOMMENDATION

5.1 Conclusion

Filler load refers to organic or inorganic substances that are put into matrix material to alter its characteristics. The various physical and mechanical characteristics of the glass-ceramic composite were influenced by the different filler load and sintering temperature applied to the glass-ceramic composite. As a result, the use of cockle shell as a filler in glass composites has been studied. Experimentation and testing comprising physical characteristics, material characterization, mechanical properties, and acoustic measurement were performed to meet the significant objectives of this study. The resulting outcome is related to the different sintering temperatures employed. In this study, sintering temperatures of 700, 750, 800, and 850 ° C were employed. This chapter presents the findings of a study on batch formulations of glass-ceramic composite at different sintering temperatures:

- a) The colour shift can be utilized as a visual indicator that crystalline precipitation has occurred. The colour variations happened as the sintering temperature increased. Diffusion leads to the different sintering behaviour on the GCC surface. For the linear shrinkage, the dimension is shrunk when the samples without CS filler loading at all temperatures. Only 30wt.% of the CS filler load can minimise porosity, which causes shrinkage during the GCC sintering process. As a result, the porosity created during the sintering process resulted in a larger percentage of apparent porosity on samples with 40 and 50wt.% CS filler load. The density of 30wt.% of CS filler loading at 700 and 850°C have the same value of 2.31g/cm³. Because the Cs filler was totally fused into the SLSG, it exhibited decreased porosity created in the structure of 30wt.% CS filler load.

- b) The microhardness of the glass composite displays that formulation of the composite with 30wt.% of CS filler loading sintered at 850°C has the highest value, which is 1004.86Hv. It can be concluded that at 850°C, the hardness increased approximately 38% ($613.58 / (613.58 + 1004.86)$) from 613.58 to 1004.84 compared to samples sintered at 700°C and this composition with 850°C, value density also high which supported the value of hardness. By using acoustic measurement, Young's modulus can be approximately calculated. Unfortunately, for 40 and 50wt.% of CS filler load, Young's modulus value cannot be calculated due to the samples has been shattered. But from what can be concluded, the trend cannot be compared due to the inconsistency of the data.
- c) Surface morphology cannot be done due to unforeseen issue during the laboratory works. Hence the comparison of the surface morphology from past literatures conclude that, when the sintering temperature increasing, the micropores decreased.

5.2 Recommendation

In this work, the identification was explored in order to offer critical information about the glass-ceramic composite. Thus, more research is needed to learn more about the cockle shell as a filler in the glass-ceramic composite. The following are suggestions for the future:

- It is critical to study the inclusion of binder throughout the manufacturing process of the green body. This effort will contribute to the enhancement of the physical and mechanical characteristics of the glass composite.
- For the pressed mould, it is suggested to use a pellet mould due to the pressure distribution. This is because, the pressure on the square mould is not uniformly distributed resulting in the inconsistency data in microhardness.

5.3 Life Long Learning Element

Life long learning can be defined as the ongoing growth of knowledge and abilities that people experience after completing formal education and throughout their lives and able to apply the knowledge in reality. The knowledge that has been gained through this study is

to develop an understanding of the element in eco-waste materials to use as substitutes material in any application.



REFERENCE

- Almasri, K. A., Sidek, H. A. A., Matori, K. A., & Zaid, M. H. M. (2017). Effect of sintering temperature on physical, structural and optical properties of wollastonite based glass-ceramic derived from waste soda lime silica glasses. *Results in Physics*, 7, 2242–2247. <https://doi.org/10.1016/J.RINP.2017.04.022>
- Arcaro, S., Moreno, B., Chinarro, E., Salvador, M. D., Borrell, A., Nieto, M. I., Moreno, R., & de Oliveira, A. P. N. (2017). Properties of LZS/nanoAl₂O₃ glass-ceramic composites. *Journal of Alloys and Compounds*, 710, 567–574. <https://doi.org/10.1016/j.jallcom.2017.03.299>
- ASTM E494 - 95 Standard Practice for Measuring Ultrasonic Velocity in Materials. (n.d.). Retrieved June 20, 2021, from <https://www.astm.org/DATABASE.CART/HISTORICAL/E494-95.htm>
- Ayob, N. F., Juoi, J. M., Rosli, Z. M., & Rosli, N. R. (2011). Characterisation and properties of sintered glass-ceramics produced from recycling glass by using pressure-less method. *Key Engineering Materials*, 471–472(October 2018), 933–938. <https://doi.org/10.4028/www.scientific.net/KEM.471-472.933>
- Barros, M. C., Bello, P. M., Bao, M., & Torrado, J. J. (2009). From waste to commodity: transforming shells into high purity calcium carbonate. *Journal of Cleaner Production*, 17(3), 400–407. <https://doi.org/10.1016/j.jclepro.2008.08.013>
- Ben Ghorbal, G., Tricoteaux, A., Thuault, A., Louis, G., & Chicot, D. (2017). Comparison of conventional Knoop and Vickers hardness of ceramic materials. *Journal of the European Ceramic Society*, 37(6), 2531–2535. <https://doi.org/10.1016/J.JEURCERAMSOC.2017.02.014>
- Berger, B. (2010). The Importance and Testing of Density / Porosity / Permeability / Pore Size for Refractories. *Refractories*, 111–116.
- Cattell, M. J., Patzig, C., Bissasu, S., Tsoutsos, A., & Karpukhina, N. (2020). *Nucleation efficacy and flexural strength of novel leucite glass-ceramics*. <https://doi.org/10.1016/j.dental.2020.03.017>

- Chinnam, R. K., Bernardo, E., Will, J., & Boccaccini, A. R. (2015). Processing of porous glass ceramics from highly crystallisable industrial wastes. *Https://Doi.Org/10.1179/1743676115Y.0000000053*, 114, S11–S16. <https://doi.org/10.1179/1743676115Y.0000000053>
- Chinnam, R. K., Francis, A. A., Will, J., Bernardo, E., & Boccaccini, A. R. (2013). Review. Functional glasses and glass-ceramics derived from iron rich waste and combination of industrial residues. In *Journal of Non-Crystalline Solids* (Vol. 365, Issue 1, pp. 63–74). North-Holland. <https://doi.org/10.1016/j.jnoncrysol.2012.12.006>
- Dermawan, A. (2021). *Malaysia to produce 150,000 metric tonnes of cockles by 2025*. <https://www.nst.com.my/news/nation/2021/05/687587/malaysia-produce-150000-metric-tonnes-cockles-2025>
- Deubener, J., Allix, M., Davis, M. J., Duran, A., Höche, T., Honma, T., Komatsu, T., Krüger, S., Mitra, I., Müller, R., Nakane, S., Pascual, M. J., Schmelzer, J. W. P., Zanotto, E. D., & Zhou, S. (2018). Updated definition of glass-ceramics. *Journal of Non-Crystalline Solids*, 501(February), 3–10. <https://doi.org/10.1016/j.jnoncrysol.2018.01.033>
- Ermrich, M., & Opper, D. (2011). XRD for the analyst: getting acquainted with the principles. In *PANalytical*.
- Francis Thoo, V. W., Zainuddin, N., Matori, K. A., & Abdullah, S. A. (2013). Studies on the potential of waste soda lime silica glass in glass ionomer cement production. *Advances in Materials Science and Engineering*, 2013. <https://doi.org/10.1155/2013/395012>
- Franco, E. E., Buiochi, F., & Meza, J. M. (2011). *Measurement of elastic properties of materials by the ultrasonic through-transmission technique*. 78(168), 58–64. <http://www.redalyc.org/articulo.oa?id=49622401007>
- George, P., Hamid, Z. A., Zakaria, M. Z. A. B., Perimal, E. K., & Bharatham, H. (2019). A short review on cockle shells as biomaterials in the context of bone scaffold fabrication. *Sains Malaysiana*, 48(7), 1539–1545. <https://doi.org/10.17576/jsm-2019-4807-23>
- Gualberto, H. R., Lopes, R. S., Silva, F. A. N. G. D. N. G., Schnurr, E., Poiate Junior, E., Andrade, M. C. D., Junior, E. P., & Andrade, C. De. (2019). Influence of Sintering Temperature on Mechanical Properties of Glass-Ceramics Produced with Windshield

- Waste. *International Journal of Chemical Engineering*, 2019, 8–10. <https://doi.org/10.1155/2019/2531027>
- Guan, K., Qin, W., Liu, Y., Yin, X., Peng, C., Lv, M., Sun, Q., & Wu, J. (2016). Evolution of porosity, pore size and permeate flux of ceramic membranes during sintering process. *Journal of Membrane Science*, 520, 166–175. <https://doi.org/10.1016/J.MEMSCI.2016.07.023>
- Hasanuzzaman, M., Rafferty, A., Sajjia, M., & Olabi, A.-G. (2016). Properties of Glass Materials. In *Reference Module in Materials Science and Materials Engineering*. Elsevier. <https://doi.org/10.1016/b978-0-12-803581-8.03998-9>
- Hazurina, N. O. R., Bakar, A. B. U., Johari, M., & Don, M. A. T. (2012). Potential Use of Cockle (*Anadara granosa*) Shell Ash as Partial Cement Replacement in Concrete. *AWAM International Conference on Civil Engineering & Geohazard Information Zonation (AICCE'12)*, 2(August), 369–376.
- Hisham, N. A. N., Zaid, M. H. M., Aziz, S. H. A., & Muhammad, F. D. (2021). Comparison of foam glass-ceramics with different composition derived from ark clamshell (ACS) and soda lime silica (SLS) glass bottles sintered at various temperatures. *Materials*, 14(3), 1–14. <https://doi.org/10.3390/ma14030570>
- Höland, W., & Beall, G. H. (2019). Glass-ceramic technology. In *Glass-Ceramic Technology* (3rd ed.). Wiley-American Ceramic. <https://doi.org/10.1002/9781119423737>
- Jassim, A. K. (2017). Sustainable Solid Waste Recycling. *Skills Development for Sustainable Manufacturing*, 1–16. <https://doi.org/10.5772/intechopen.70046>
- Jusoh, W. N. W., Matori, K. A., Zaid, M. H. M., Zainuddin, N., Khiri, M. Z. A., Rahman, N. A. A., Jalil, R. A., & Kul, E. (2019a). Effect of sintering temperature on physical and structural properties of Alumino-Silicate-Fluoride glass ceramics fabricated from clam shell and soda lime silicate glass. *Results in Physics*, 12, 1909–1914.
- Jusoh, W. N. W., Matori, K. A., Zaid, M. H. M., Zainuddin, N., Khiri, M. Z. A., Rahman, N. A. A., Jalil, R. A., & Kul, E. (2019b). Effect of sintering temperature on physical and structural properties of Alumino-Silicate-Fluoride glass ceramics fabricated from

- clam shell and soda lime silicate glass. *Results in Physics*, 12, 1909–1914. <https://doi.org/10.1016/J.RINP.2019.01.077>
- Kang, S.-J. L. (2005). SINTERING PROCESSES. In *Sintering* (pp. 3–8). Elsevier. <https://doi.org/10.1016/b978-075066385-4/50001-7>
- Karazi, S. M., Ahad, I. U., & Benyounis, K. Y. (2017). Laser Micromachining for Transparent Materials. In *Reference Module in Materials Science and Materials Engineering*. Elsevier. <https://doi.org/10.1016/b978-0-12-803581-8.04149-7>
- Khemthong, P., Luadthong, C., Nualpaeng, W., Changsuwan, P., Tongprem, P., Viriya-Empikul, N., & Faungnawakij, K. (2012a). Industrial eggshell wastes as the heterogeneous catalysts for microwave-assisted biodiesel production. *Catalysis Today*, 190(1), 112–116. <https://doi.org/10.1016/j.cattod.2011.12.024>
- Khemthong, P., Luadthong, C., Nualpaeng, W., Changsuwan, P., Tongprem, P., Viriya-Empikul, N., & Faungnawakij, K. (2012b). Industrial eggshell wastes as the heterogeneous catalysts for microwave-assisted biodiesel production. *Catalysis Today*, 190(1), 112–116. <https://doi.org/10.1016/j.cattod.2011.12.024>
- Khiri, M. Z. A., Matori, K. A., Zaid, M. H. M., Abdullah, A. C., Zainuddin, N., Jusoh, W. N. W., Jalil, R. A., Rahman, N. A. A., Kul, E., Wahab, S. A. A., & Effendy, N. (2020). Soda lime silicate glass and clam Shell act as precursor in synthesize calcium fluoroaluminosilicate glass ionomer cement with different ageing time. *Journal of Materials Research and Technology*, 9(3), 6125–6134. <https://doi.org/10.1016/j.jmrt.2020.04.015>
- Kim, K. H., Ong, J. L., & Okuno, O. (2002). The effect of filler loading and morphology on the mechanical properties of contemporary composites. *Journal of Prosthetic Dentistry*, 87(6), 642–649. <https://doi.org/10.1067/mpr.2002.125179>
- Leenakul, W., Tunkasiri, T., Tongsir, N., Pengpat, K., & Ruangsuriya, J. (2016). Effect of sintering temperature variations on fabrication of 45S5 bioactive glass-ceramics using rice husk as a source for silica. *Materials Science and Engineering: C*, 61, 695–704. <https://doi.org/10.1016/J.MSEC.2015.12.029>
- Mark, U. C., Madufor, I. C., Obasi, H. C., & Mark, U. (2020). Influence of filler loading on the mechanical and morphological properties of carbonized coconut shell particles

- reinforced polypropylene composites. *Journal of Composite Materials*, 54(3), 397–407. <https://doi.org/10.1177/0021998319856070>
- Mesri, M., Shamsudin, Z., Hasan, R., & Daud, N. (2020a). Effects of bentonite and eggshell as fillers on thermal-physical properties of sintered glass composite. *Journal of Advanced Research in Fluid Mechanics and Thermal Sciences*, 66(2), 145–157.
- Mesri, M., Shamsudin, Z., Hasan, R., & Daud, N. (2020b). Effects of Bentonite and Eggshell as Fillers on Thermal-Physical Properties of Sintered Glass Composite. *Journal of Advanced Research in Fluid Mechanics and Thermal Sciences Journal Homepage*, 66, 145–157. www.akademiabaru.com/arfmts.html
- Mo, K. H., Alengaram, U. J., Jumaat, M. Z., Lee, S. C., Goh, W. I., & Yuen, C. W. (2018). Recycling of seashell waste in concrete: A review. In *Construction and Building Materials* (Vol. 162, pp. 751–764). Elsevier Ltd. <https://doi.org/10.1016/j.conbuildmat.2017.12.009>
- Moghanizadeh, A. (2021). Using Ultrasonic Tactile Sensor for Materials Recognition On Thin Wall Objects in Assembly Lines. *Journal of Artificial Intelligence in Electrical Engineering*, 5(November 2016).
- Moghanizadeh, A., & Farzi, A. (2016). Effect of heat treatment on an aisi 304 austenitic stainless steel evaluated by the ultrasonic attenuation coefficient. *Mechanical Testing/Materialography*, 58(5), 448–452. <https://doi.org/10.3139/120.110878>
- Mohamed, M., Yousuf, S., & Maitra, S. (2012). Decomposition study of calcium carbonate in cockle shell. *Journal of Engineering Science and Technology*, 7(1), 1–10.
- Munusamy, Y., Sethupathi, S., & Choon, C. H. (2019). Potential use of waste cockle shell as filler for thermoplastic composite. *Journal of Material Cycles and Waste Management*, 21(5), 1063–1074. <https://doi.org/10.1007/s10163-019-00867-9>
- Murayama, Y., Constantinou, C. E., & Omata, S. (2004). Micro-mechanical sensing platform for the characterization of the elastic properties of the ovum via uniaxial measurement. *Journal of Biomechanics*, 37(1), 67–72. [https://doi.org/10.1016/S0021-9290\(03\)00242-2](https://doi.org/10.1016/S0021-9290(03)00242-2)

- Muthusamy, K., Sabri, N. a, Resources, E., & Razak, L. T. (2012). Cockle Shell : A Potential Partial Coarse Aggregate Replacement In Concrete. *International Journal of Science, Environment and Technology*, 1(4), 260–267.
- Noor, A. H. M., Aziz, S. H. A., Rashid, S. S. A., Zaid, M. H. M., Zaripah, N. A., & Matori, K. A. (2015). Synthesis and characterization of wollastonite glass-ceramics from eggshell and waste glass. *Journal Of Solid Satate Sciences & Technology*, 16(1–2), 1–5.
- Onuoha, C., Onyemaobi, O. O., Anyakwo, C. N., & Onuegbu, G. C. (2017). Effect of Filler Content and Particle Size on the Mechanical Properties of Corn Cob Powder Filled Recycled Polypropylene Composites. *American Journal of Engineering Research (AJER)*, 6(4), 72–79.
- Phani, K. K. (2007). Estimation of elastic properties of porous ceramic using ultrasonic longitudinal wave velocity only. *Journal of the American Ceramic Society*, 90(7), 2165–2171. <https://doi.org/10.1111/j.1551-2916.2007.01736.x>
- Pinckney, L. R. (2001). Glass Ceramics. In *Encyclopedia of Materials: Science and Technology* (pp. 3535–3540). Elsevier. <https://doi.org/10.1016/B0-08-043152-6/00629-X>
- Popelka, A., Zavahir, S., & Habib, S. (2020). Morphology analysis. *Polymer Science and Innovative Applications*, 21–68. <https://doi.org/10.1016/B978-0-12-816808-0.00002-0>
- Rahaman, M. N. (2014). Bioactive ceramics and glasses for tissue engineering. In *Tissue Engineering Using Ceramics and Polymers: Second Edition*. <https://doi.org/10.1533/9780857097163.1.67>
- Rahman, N. A. A., Matori, K. A., Zaid, M. H. M., Zainuddin, N., Aziz, S. A., Khiri, M. Z. A., Jalil, R. A., & Jusoh, W. N. W. (2019). Fabrication of Alumino-Silicate-Fluoride based bioglass derived from waste clam shell and soda lime silica glasses. *Results in Physics*, 12, 743–747. <https://doi.org/10.1016/j.rinp.2018.12.035>
- Sahari, F., & Mijan, N. A. (2011). Cockle Shell As An Alternative Construction Material For Artificial Reef. *International Conference on Creativity and Innovation for Sustainable Development, September*.

- Salleh, N., Shamsudin, Z., Juoi, J. M., & Mustafa, Z. (2017). Effects of heating rates and SBE loading on sintered properties of spent bleach earth/recycled glass composite. *Journal of Mechanical Engineering and Sciences*, 11(4), 3104–3115. <https://doi.org/10.15282/jmes.11.4.2017.13.0279>
- Saparuddin, D. I., Noor Hisham, N. A., Aziz, S. A., Matori, K. A., Honda, S., Iwamoto, Y., & Mohd Zaid, M. H. (2020). Effect of sintering temperature on the crystal growth, microstructure and mechanical strength of foam glass-ceramic from waste materials. *Journal of Materials Research and Technology*, 9(3), 5640–5647. <https://doi.org/10.1016/j.jmrt.2020.03.089>
- Shamsudin, Z., Mustafa, Z., & Abd, T. (2019). *Preliminary Investigation on the Physical Properties and Morphological of Sintered Cockle Shell/ Recycled Soda Lime Silicate Composite*. <https://www.researchgate.net/publication/334259943>
- Shamsudin, Z., Razali, A. H., Suzaim, F. H., Mustafa, Z., Rahim, T. A., & Hodzic, A. (2018). Preliminary investigation on the physical properties and morphological of sintered cockle shell/recycled soda lime silicate composite. *Journal of Advanced Manufacturing Technology*, 12(Specialissue3), 125–138.
- Sindhu, R., Binod, P., & Pandey, A. (2015). Microbial Poly-3-Hydroxybutyrate and Related Copolymers. *Industrial Biorefineries and White Biotechnology*, 575–605. <https://doi.org/10.1016/B978-0-444-63453-5.00019-7>
- Sohn, H. Y., & Olivias-Martinez, M. (2014). Lead and Zinc Production. In *Treatise on Process Metallurgy* (Vol. 3, pp. 671–700). Elsevier Ltd. <https://doi.org/10.1016/B978-0-08-096988-6.00025-0>
- Van Nguyen, C., Sistla, S. K., Van Kempen, S., Giang, N. A., Bezold, A., Broeckmann, C., & Lange, F. (2016). A comparative study of different sintering models for Al₂O₃. *Journal of the Ceramic Society of Japan*, 124(4), 301–312. <https://doi.org/10.2109/jcersj2.15257>
- Wang, J., Liu, E., & Li, L. (2019). Characterization on the recycling of waste seashells with Portland cement towards sustainable cementitious materials. *Journal of Cleaner Production*, 220, 235–252. <https://doi.org/10.1016/j.jclepro.2019.02.122>

- Wowk, D., & Marsden, C. (2018). The effects of test set-up on the apparent flexural modulus of thin angle-ply laminates using standard four-point bend testing. *International Journal of Computational Methods and Experimental Measurements*, 6(3), 551–562. <https://doi.org/10.2495/CMEM-V6-N3-551-562>
- Wypych, G. (2016). THE EFFECT OF FILLERS ON THE MECHANICAL PROPERTIES OF FILLED MATERIALS. In *Handbook of Fillers* (pp. 467–531). Elsevier. <https://doi.org/10.1016/b978-1-895198-91-1.50010-5>
- Yang, D., Zhang, Y., Song, X., Chen, Y., Shen, Z., & Yang, C. (2016). Effects of sintering temperature and holding time on porosity and shrinkage of glass tubes. *Ceramics International*, 5(42), 5906–5910. <https://doi.org/10.1016/J.CERAMINT.2015.12.138>
- Yoon, G. L., Kim, B. T., Kim, B. O., & Han, S. H. (2003). Chemical-mechanical characteristics of crushed oyster-shell. *Waste Management*, 23(9), 825–834. [https://doi.org/10.1016/S0956-053X\(02\)00159-9](https://doi.org/10.1016/S0956-053X(02)00159-9)
- Zaid, M. H. M., Matori, K. A., Wah, L. C., Sidek, H. A. A., Halimah, M. K., Wahab, Z. A., & Azmi, B. Z. (2011). Elastic moduli prediction and correlation in soda lime silicate glasses containing ZnO. *International Journal of the Physical Sciences*, 6(6), 1404–1410. <https://doi.org/10.5897/IJPS11.111>
- Zawrah, M. F., Khattab, R. M., El-Kheshen, A. A., & el Fadaly, E. (2017). Sintering and properties of borosilicate glass/Li-Na-K-feldspar composites for electronic applications. *Ceramics International*, 43(17), 15068–15073. <https://doi.org/10.1016/J.CERAMINT.2017.08.033>

APPENDICES

A Gantt Chart for FYP 1

No	Project Description	Week 1	Week 2	Week 3	Week 4	Week 5	Week 6	Week 7	Week 8	Week 9	Week 10	Week 11	Week 12	Week 13	Week 14	Week 15
1	Registration for PSM Title and Supervisor															
2	First Briefing of title															
3	Searching for related journals/articles/thesis															
4	Chapter 1: Introduction															
5	Chapter 2: Literature Review															
6	Chapter 3: Methodology															
7	Abstract															
8	Table of content															
9	References															
10	Logbook submission															
11	Online presentation and Q&A session															
12	FYP 1 report submission															

B Gantt Chart for FYP 2

TASK	WEEK														
	1	2	3	4	5	6	7	8	9	10	11	12	13	14	
Planning for PSM 2 project															
PSM 2 Briefing															
PSM 1 report amendment															
Discussion with Supervisor for Project Procedure															
Sample Preparation: Crushing and sieving SLSG waste and CS waste															
Sample Preparation: Calcination process at 1000°C with a heating rate 10°C/min for 4 hours															
FT-IR Analysis															
Sample Preparation: Pressing the SLSG powder and CS powder															
Sinter the powder at 700, 750, 800 and 850°C with a heating rate 2°C/min for 1 hour.															
Ultrasonic Test															

